SCUOLA DI SCIENZE
Dipartimento di Chimica Industriale “Toso Montanari”

Corso di Laurea Magistrale in

Chimica Industriale

Classe LM-71 - Scienze e Tecnologie della Chimica Industriale

Online monitoring of gas-liquid dispersion in a tubular reactor using passive acoustic emission

Tesi di laurea sperimentale

CANDIDATA

Lisa Della Vecchia

RELATORE

Prof. Federico Alberini

CORRELATORE

Chiar.mo Prof. Alessandro Paglianti

Anno Accademico 2023-2024

Abstract

Climate change is one of the most pressing challenges facing our planet today. It is characterized by rising temperatures, disrupted weather patterns and profound environmental impacts. The accumulation of greenhouse gases (GHGs) in the Earth's atmosphere, with water vapor, CO_2, CH_4 and ozone being the main contributors, is the main catalyst for this phenomenon. In view of the significant greenhouse effect associated with CO_2 and CH_4, the search for efficient utilization routes for these gases is of paramount importance.

There are a number of strategies to reduce the level of CO_2 in the atmosphere, with the main focus on the capture, sequestration and storage of CO_2. However, in order to significantly reduce overall emissions, it is equally important to achieve a zero-emissions pathway.

In this context, industrial chemistry plays a fundamental role, as it has the task of researching new strategies to reduce greenhouse gas emissions and control these processes with extreme efficiency.

The present work fits into this scenario by studying an innovative control system based on the recording and subsequent processing of passive acoustic emissions generated inside the tube: in fact, every phenomenon in the process generates emissions. This is a strong point for the future, as it is a non-invasive sensor, which is therefore positioned outside the tube, is very precise and provides data in real time.

The aim for the future is to combine this analysis system with the programming of machine learning, a branch of artificial intelligence that brings together methods developed in the last decades of the 20th century in different scientific communities under different names such as: computational statistics, pattern recognition, artificial neural networks, adaptive filtering, dynamic systems theory, image processing, data mining and adaptive algorithms; it uses statistical methods to improve the performance of an algorithm in identifying patterns in data.

Literature review

1. Chemical reactors

Chemical processes may be classified as batch, continuous, or semibatch and as either steady-state or transient. All real reactors fall within the spectrum bounded by ideal semibatch and continuous reactors, meaning they exhibit a combination of segregation and mixing. Knowing the extent of each allows for the design of the actual reactors.

1.1 Tubular reactor

A tubular reactor, also known as Plug Flow Reactor (PFR), provides a continuous flow of matter in and out of the system and it is schematically illustrated as in *Figure 1*[1]:

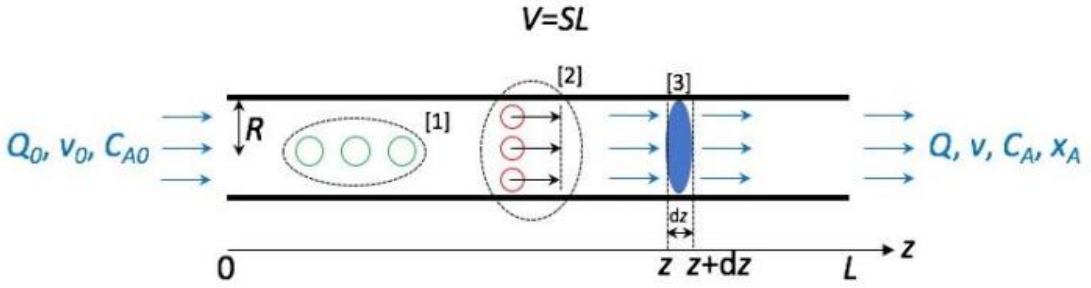

FIGURE 1 - SCHEME OF TUBULAR REACTOR, WHERE [1] REPRESENTS FLUID ELEMENTS POSITIONED AT DIFFERENT VALUES OF *Z*, EACH CHARACTERIZED BY ITS OWN CONVERSION X_A. [2] ARE FLUID ELEMENTS POSITIONED AT THE SAME VALUES OF *Z*, BUT AT DIFFERENT RADIAL COORDINATES, THEY ALSO HAVE THE SAME CONVERSION X_A AND AXIAL VELOCITY. [3] REPRESENTING THE CROSS-SECTION AREA. Q_0, v_0, C_{A0} ARE RESPECTIVELY THE FLOW RATE, THE VELOCITY AND THE CONCENTRATION AT THE BEGINNING. Q, v, C_A CORRESPOND TO THE FLOW RATE, THE VELOCITY AND THE CONCENTRATION IN THE END. R IS THE PIPE RADIUS.

The primary direction of motion is defined and represented by the symbol z, where z=0 denotes the inlet and z=l the outlet and the reactor has a length equal to L.

The premise of perfect axial segregation serves as a PFR's initial foundational assumption. Considering the axis as the main axis of motion, which is the z-axis, three fluid elements are taken at different values along the axis: there is no interaction between the fluid elements, diffusive and therefore chaotic motions are excluded, but there are only purely convective motions. There is no diffusion, no random walk and no back mixing. Therefore, each element

of fluid along the axis preserves its properties, there is no mixing of matter and no thermal mixing[2].

The piston flow hypothesis also suggests perfect radial mixing. Considering three fluid elements positioned at the same radial height, to assert perfect mixing means to acknowledge the prevalence of diffusive motion, consequently, there is uniformity in intensive properties, such as the degree of conversion[3]. In other words, if an analysis reveals a specific conversion degree for one element, the corresponding elements along the radial direction will exhibit the same degree. Fluid elements become indistinguishable from each another as they have identical chemical compositions. Furthermore, elements aligned along the radical coordinate possess identical velocity vector.

In the context of the piston flow hypothesis, this results in what is known as flat velocity profile. This signifies that mixing along the radius is so effective that the fluid elements become indistinguishable.

The residence time of the fluid elements in the reactor is also a determining factor. Calculating the space-time of a reactor is crucial as it necessities the calculation of the reactor's volume. By understanding the flow rate and incorporating time, this calculation can be effectively performed. So, it guarantees the ability to meet production or processing requirements.

1.2 Batch and semibatch reactor

The batch reactor, also known as a STR (Stirred Tank Reactor), operates as a perfectly mixed and discontinuous system. In this reactor, substances are not continuously introduced or removed; instead, the reactor is filled at the start of the reaction and subsequently emptied at the end of the process [4].

From a fluid dynamics perspective, the fact that the reactor is perfectly mixed implies that intensive properties are uniform in space at a fixed point in time.

In contrast, the perfectly mixed tank reactor CSTR (Continuous Stirred Tank Reactor) is similar to the STR but with an inflow and an outflow stream. Here, not only are the properties uniform in the space, but also remain constant over time, meaning they always correspond to the values at the reactor outlet. This implies that when a fluid element enters the reactor, it

instantly equilibrates with the outlet properties. Consequently, its conversion level will consistently be x_A final and the entering reactant concentration will promptly decrease to final concentration.

1.3 Comparison between batch, semibatch and tubular reactor

The distinction between the Stirred Tank Reactor and the Plug Flow Reactor lies in their operational nature: the former is discontinuous, while the latter is continuous. Comparing the two continuous reactors, it is evident that a fluid element is more inclined to undergo reaction in a Plug Flow Reactor (PFR) rather than in a Continuous Stirred Tank Reactor (CSTR). In the latter case, the fluid element, throughout its entire lifespan, remains at the outlet conversion level. Consequently, since there is a one-to-one correspondence between conversion level and reaction rate, if the fluid element is confined to a single conversion level, it experiences only one reaction rate. This rate is the least favorable because if the fluid element operates in the CSTR at a high, i.e., final, value of x_A, it implies that the concentration of the limiting reactant is low. When the concentration of the limiting reactant is low, the reaction rate is also low, particularly being the worst among all possible rates[5].

In a PFR, the fluid element undergoes variations across the infinite range of conversion levels between the inlet and outlet. Consequently, it experiences an array of reaction rates encompassing all possible values within this continuum. In contrast, in a CSTR, the fluid element is confined to a single conversion level, thereby subjected to only one reaction rate. As a result, the average reaction rate in the PFR, considering the entire spectrum of conversion levels, is higher, making it a more favorable scenario.

1.4 Tubular reactor applications

A tubular reactor can be adapted for absorption processes, providing an effective method of CO_2 capture in various industrial applications.

The most effective method to lower atmospheric carbon dioxide levels is by decreasing fossil fuel consumption[6]. Nevertheless, this is a challenging goal to accomplish because many industrial facilities and power plants are designed to rely on fossil fuels. As a result, carbon capture and storage (CCS) technologies have been developed and implemented in numerous facilities around the world[7]. These CCS technologies come in various forms, with one of the

most commonly used being the wet absorption technique, which employs a liquid absorbent to capture carbon dioxide[8].

In this approach, a liquid absorbent such as amine, which has a high reactivity with gaseous carbon dioxide, captures CO_2 and becomes saturated at the absorber. The CO_2-laden amine is then moved to a desorber, where the absorbed carbon dioxide is separated from the liquid absorbent at a relatively high temperature. The absorbent is then regenerated and transported back to the absorber, creating a continuous cycle. Monoethanolamine (MEA) is a commonly used absorbent due to its high reaction rate with carbon dioxide, forming carbonate and carbamate ions[9,10]. This outlines the basic principle of traditional wet absorption CCS technology. However, because regenerating the absorbent requires significant energy, the overall energy consumption of the continuous absorption–desorption process is substantial[10,11]. To address this issue, researchers have explored methods to eliminate the desorption step. One promising technique involves separating dissolved carbon dioxide by converting it into precipitated salts through chemical reactions[12].

Figure 2 shows the simplified process map for simultaneous ammonium nitrate and calcium oxide processes.

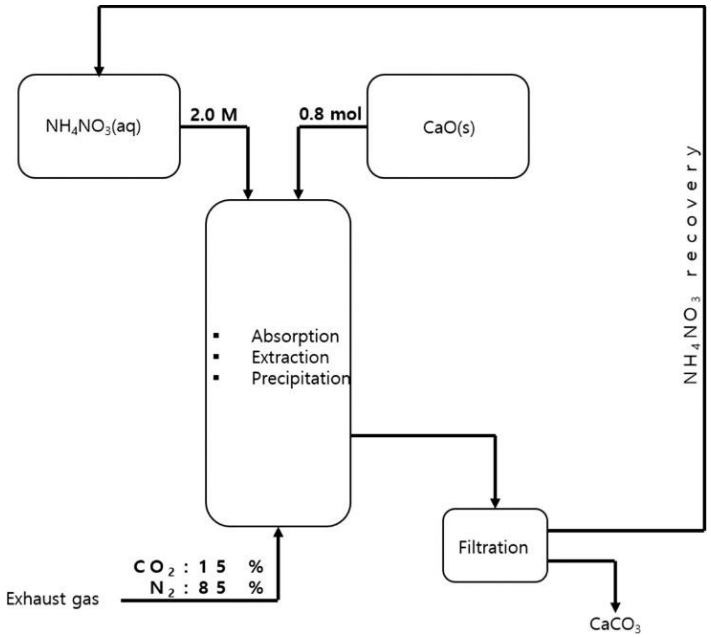

FIGURE 2 - DIAGRAM OF A LIQUID GAS TUBULAR REACTOR FOR CO_2 ABSORPTION[13]

As mentioned above, the carbon capture and utilization process with several key features has been developed, including absorbent recycling, calcium carbonate salt precipitation, and the elimination of the desorption step[14].

Each step and the entire process are outlined below:

Step 1: Mixing ammonium nitrate solution with solid calcium oxide.

Step 2: Carbon dioxide absorption into the solution at step 1.

Step 3: Separating precipitated calcium carbonate salt from the solution at step 2.

Step 4: Through steps 1–3, absorbent solution is regenerated and whole process is repeated.

Aqueous ammonium nitrate solution mixed with calcium oxide are used as absorbents.

2. The role of chemical industry in climate change

Climate change stands out as one of the most urgent challenges confronting our planet today, marked by escalating temperatures, disrupted weather patterns, and profound environmental repercussions. The primary catalyst for this phenomenon is the buildup of greenhouse gases (GHGs) in the Earth's atmosphere, with water vapor, CO_2, CH_4, and ozone being the key contributors. Given the substantial greenhouse effect associated with CO_2 and CH_4, exploring efficient utilization routes for these gases is of paramount importance.

Various strategies exist to mitigate CO_2 levels in the atmosphere, with a predominant focus on capturing, sequestering, and storing CO_2. However, achieving an emission-free pathway is equally crucial to significantly decrease overall emissions.

The pathways for carbon capture derived from three potential sources are given in *Figure 3*[15]:

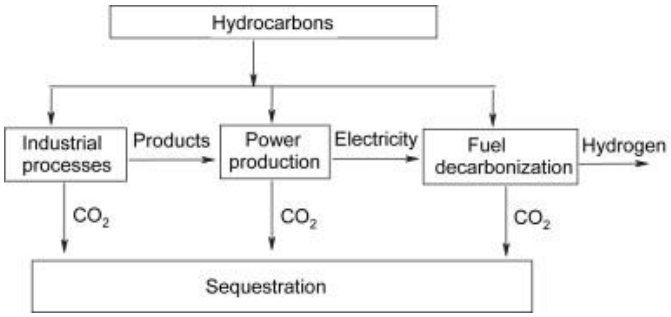

FIGURE 3 -SOURCES OF CO_2 FOR SEQUESTRATION

The achievement of carbon capture and separation from significant point sources, such as power plants, hinges on ongoing research, development, and demonstration efforts. It is crucial to conduct research aimed at developing technologies and processes that not only enhance the efficiency of capture systems but also reduce overall costs and improve energy efficiency. This research is essential for creating a practical plan for greenhouse gas (GHG) control implementation, which should encompass not only power plants and industrial facilities but also the necessary infrastructure to support such implementation[15].

The growing societal awareness of the environmental impact of human activities, coupled with a commitment to reducing pollution and energy waste, has spurred the scientific community into action. Numerous disciplines are now directing their research efforts toward a more sustainable approach[16].

Within this context, chemical industry emerges as a pivotal player, shouldering a significant responsibility and poised to play a crucial role in the collective effort to combat global warming.

2.1 Why capture CO_2

Human factors are one of the key contributors to carbon dioxide emissions into the environment.

When greenhouse gases such as carbon dioxide, perfluorocarbons (PFCs), methane, nitrous oxide, and chlorofluorocarbons (CFCs) build up in the atmosphere, they obstruct the Earth's ability to emit terrestrial radiation. Of the six greenhouse gases specified in the Kyoto Protocol, carbon dioxide is present in much greater quantities in the environment compared to the others[17].

In 2023, global carbon emissions from fossil fuels have once again surged, reaching unprecedented levels. According to the annual Global Carbon Budget, projections indicate a notable increase, with fossil carbon dioxide (CO_2) emissions expected to reach 36.8 billion tons – a 1.1% rise compared to 2022. Despite a decline in fossil CO_2 emissions observed in certain regions such as Europe and the USA, the overall trend remains an upward trajectory[18].

In 2015, during the conference dedicated to discussing and negotiating global action to combat climate change, the member of states of the United Nations concluded the Paris

Agreement[19], which set targets to keep the global temperature increase below 2 degrees Celsius: to reduce the carbon dioxide (CO_2) emission intensity of the global economy by 85% over 35 year. This means reducing energy-related CO_2 emissions by an average of 2,6% per year, or 0,6 gigatons (Gt) per year in absolute terms[20].

A key mechanism for achieving this goal is the Nationally Determined Contributions (NDCs) submitted by countries under the agreement. These NDCs typically include measures to address greenhouse gas (GHG) emissions from the energy sector. The objective of reducing GHG emissions and speeding up the transition to a low-carbon energy system is closely tied to the rapid development of clean energy and material efficiency. A crucial part of this process is the increased deployment of renewable technologies[21].

Carbon capture and storage (CCS) is a promising strategy for mitigating global warming and climate change. CCS involves capturing carbon dioxide (CO_2) from industrial and transport sectors and transporting it to a regulated site for storage. This method is one of the practical approaches for reducing global warming and its impact on humanity and other living species. However, the implementation of CCS has implications for the cost of energy production and the rate at which the technology can be commercialized[22].

As the world continues to rely heavily on fossil fuels, there is a critical need for effective CO_2 capture methods from power plants, which are major sources of CO_2 emissions[23]. CO_2 capture can be applied to large power plants, involving the compression of CO_2 and its transportation to large storage sites such as the oceans[24].

In Scotland, the Captain Sandstone formation is being explored to determine its capacity and commercial viability for CO_2 storage. The Scottish Government is funding this project with an estimated cost of £290,000. Located in the Moray Firth, half a mile below the seabed and 30 miles into the North Sea, the Captain Sandstone is capable of storing CO_2 from Scotland's coal-fired power stations for decades. *Figure 4*[25] provides a detailed outline of the project.

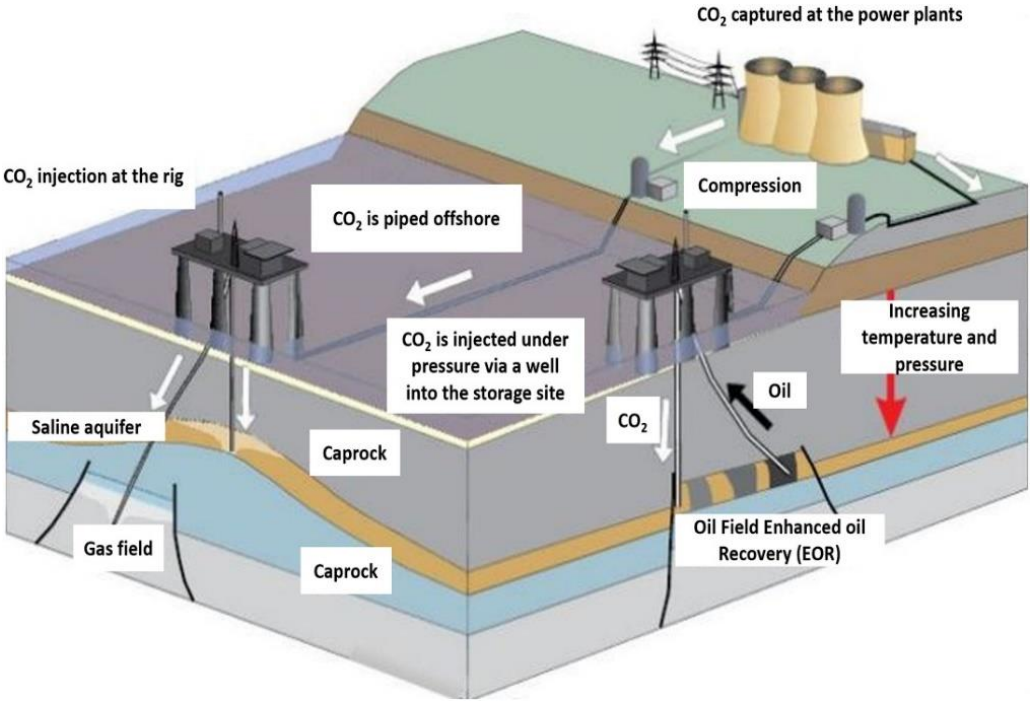

FIGURE 4 - CARBON CAPTURE AND STORAGE INFRASTRUCTURE USING GEOLOGICAL FORMATIONS

There are other options for storing CO_2 like ocean storage and industrial fixation of CO_2 into carbonates. The fraction of CO_2 captured usually determines the total reduction of emissions into the atmosphere. Currently, most CCS technologies available are able to absorb nearly 85–95% of CO_2 produced by a power plant.

Table 1 summarizes annual global CO_2 emissions from various industrial activities, highlighting the dominance of power generation, which accounts for nearly three-quarters of annual global emissions[26].

Production method	Sources	Total emissions ($MtCO_2/yr$)
Fossil products		
Power	4942	10,539
Cement production	1175	932
Refinery	638	798
Iron and steel industry	269	646
Petrochemical industry	470	379
Oil and gas processing	Not available	50
Other sources	90	33
Biomass		
Bioethanol and bioenergy	303	91
Total	7887	13,466

TABLE 1 - GLOBAL INDUSTRIAL ACTIVITIES AND TOTAL EMISSIONS YEARLY

Among various technologies, CO_2 adsorption has garnered widespread attention primarily due to its low energy requirements[27].

Through advancements in adsorbent technology, a variety of materials have been developed for carbon capture and sequestration, including zeolites, activated carbons, metal-organic frameworks, covalent organic frameworks, and silicates[28]. Generally, carbon dioxide adsorbents are categorized into two main types: physical adsorbents and chemical adsorbents. For physical adsorbents, the textural properties—such as pore size, surface area, and pore structure—are crucial for their performance. Typically, having a larger surface area and volume, with pore diameters less than 0.7 nm, enhances the adsorption process[29,30].

2.2 The absorption process

Absorption is a process by which an inert gaseous stream removes a compound gas, such as pollutants. This compound is absorbed into a liquid, which may be an aqueous solution. It is a widely used process in the environmental sector for cleaning gases from gaseous pollutants and for separation processes.

The explanation for the absorption process is the double film theory. The theory, originally proposed by Whitman, predicts a bulk consisting of both gas and liquid phases, characterized by turbulent motion and the absence of concentration gradients.

Schematically, the interface is the line that separates the two zones (*Figure 5*[31]): on the left is the gas, on the right is the liquid; the model assumes the existence of turbulent motion both in the liquid mass and in the gaseous mass; therefore, the concentrations in the two phases are equal in a given section of the apparatus: the resistance is concentrated in the liquid film and in the gaseous film, area where the concentration varies linearly. In the sine of the gas phase, the concentration of the species to be transferred A remains is amounting to *y*, and throughout the liquid mass, the concentration is equal to *x*. In reality, as with velocity in the case of mass transport and temperature in the case of energy transport, there are variations of the order of interest, in this case the concentration or partial pressure of the species A, in the turbulent core, but they are not as pronounced as in the laminar layer (which is stagnant).

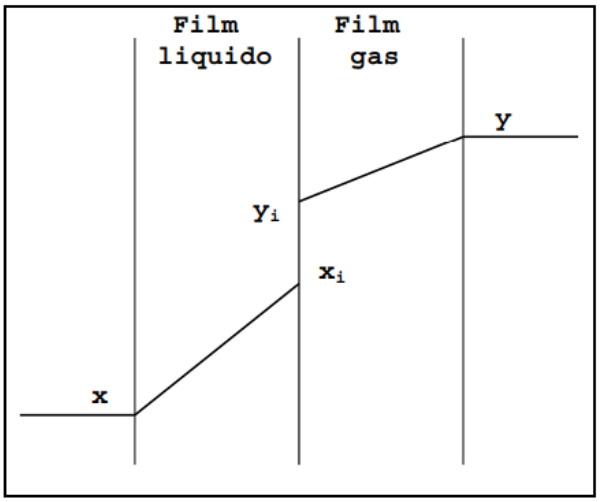

FIGURE 5 - DOUBLE FILM SCHEME.

2.3 CO_2 capture under two-phase flow conditions

The removal of CO_2 from the gas phase in liquid solvents through chemical reactions, such as chemical adsorption, the most widely used and promising CO_2 capture method[32], has been the focus of most research efforts in this context. As a result, only a limited number of studies have specifically investigated the direct solubility of CO_2 in water alone[33]. When injected into water, over 99% of the injected CO_2 dissolves in water, while less than 1% reacts

chemically with H_2O molecules to form carbonic acid (H_2CO_3)[34]. CO_2 is a valuable chemical compound and, when dissolved in water, can be used in many processes for various applications, most of which are in the food and beverage industry[35]. For example, water enriched with CO_2 is widely used in greenhouses to enhance the growth of plants, as it plays a key role in the process of photosynthesis. It is also used to grow crops and algae and for pest control. In addition, recent research has investigated the conversion of the[35] chemical energy potential of dissolved CO_2 in water into electricity using an electrochemical system (a pH gradient flow cell).

Injecting the gas into the liquid phase brings the two phases into direct contact, which can provide an effective method for mass exchange due to the direct contact between the gas and liquid phases within the riser[36]. As shown in *Figure 6*[37], the concentration difference of gas species between the liquid and gas phases creates a mass concentration gradient, which facilitates the migration of mass species between the phases. This mass transfer can be bi-directional, including transfer from the gas to the liquid, from the liquid to the gas, or even simultaneously in both directions across the gas-liquid interface. The main factor governing gas-liquid mass transfer is the dynamic behavior of the gas-liquid interface, combined with the hydrodynamic properties of the liquid phase near the interface, where a mass concentration boundary layer is formed.

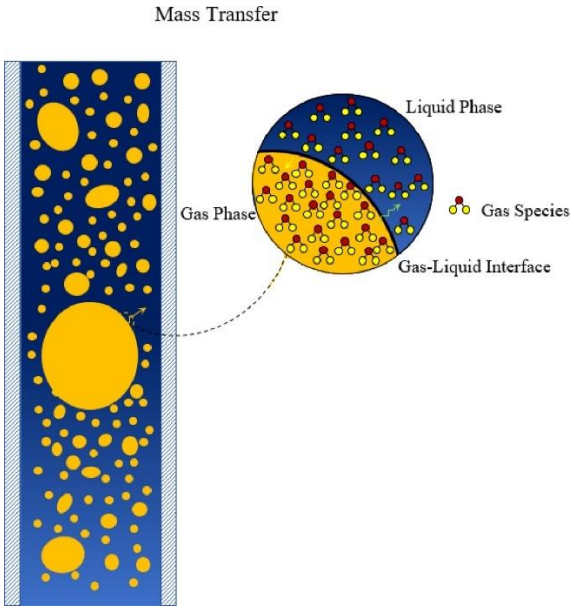

FIGURE 6 - GAS-LIQUID MASS TRANSFER AT THE GAS-LIQUID INTERFACE OF A TWO-PHASE MIXTURE.

3. Passive acoustic emission

The development of smart sensors capable to analyze data gathered on the process line and to give a real time feedback has been undergoing extensive research in the last years due to its potential benefits on the process optimization and products improvement[38].

Measurement techniques have the potential to improve system efficiency or optimize system control. One such analysis is the study of acoustic emissions. Acoustic measurements are based on the detection of ultrasonic signals[39], it can be divided into two categories: passive (acoustic emission) and active[40]. In passive measurements, the process itself generates the acoustic wave. In active measurements, an external acoustic wave is introduced into the process, and changes in its attenuation and/or velocity are typically monitored[41].

Passive acoustics involves the practice of listening for and analyzing sounds, usually within specific frequency ranges and for particular purposes.

Acoustic measurement techniques were initially invented to monitor urban infrastructure, e.g. to continuously check the condition of bridges[42], and later developed to monitor the condition of equipment and physical-chemical changes within chemical processes. A key advantage of acoustics is that it allows for non-intrusive, real-time monitoring, as it does not require direct contact with the process under investigation, but the detection sensor is mounted on the outer wall of pipes. Most research has focused on the active use of low-power ultrasound, where an acoustic wave is generated and changes in the wave are measured[43].

The speed of sound in a material is an important property to measure, as it varies with the material's physical state. Several active acoustic measurement techniques monitor the speed of sound through a material to track the progress of processes, such as polymer curing[44].

In gases, liquids and solids, acoustic waves are longitudinal, i.e. the wave energy propagates through the vibration of particles parallel to the direction of the wave, producing a series of regions of high density and high pressure (compressions) and regions of low density and low pressure (rarefactions). In solids, acoustic waves can also be transverse, where the direction of vibration of the particles is perpendicular to the direction of the wave, e.g. the vibration of a metal rod or string. The low viscosity of liquids and gases means that transverse (or shear) waves do not occur in these phases[45].

Waves are characterized and can therefore be described by their frequency, which is defined as the total number of vibrations or oscillations present in a wave in a unit of time. Frequency (f) is then related to wavelength (λ) by the law of velocity (c), i.e.:

$$c = f\lambda$$

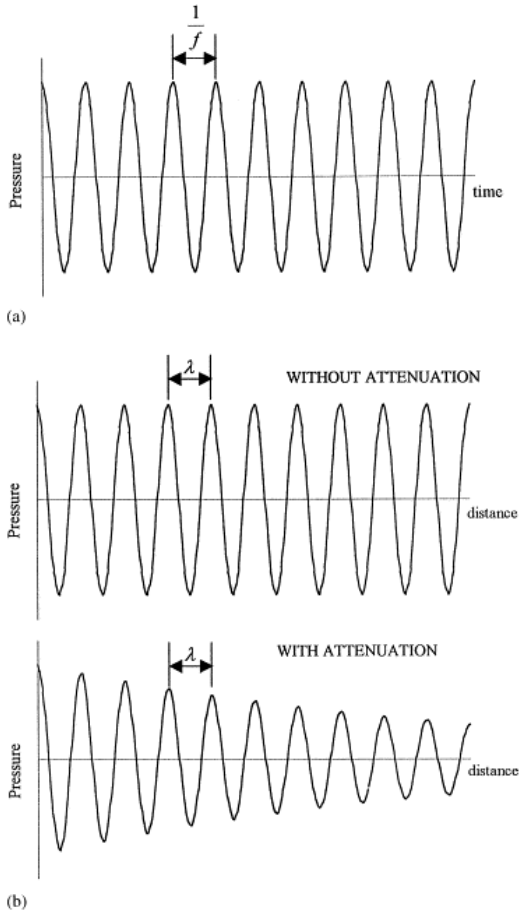

FIGURE 7 - ILLUSTRATION OF PRESSURE VARIATION DUE TO ACOUSTIC WAVES. (A) PRESSURE FLUCTUATIONS DUE AT A FIXED DISTANCE FROM A CONTINUOUS SOUND SOURCE; (B) SOUND WAVE PROPAGATION FROM A SOUND SOURCE WITH AND WITHOUT ATTENUATION.

In addition to frequency and propagation speed, an acoustic wave can also be characterized by its amplitude A. The amplitude of an acoustic wave is a function of time and the distance from the sound source at which it is measured. When an acoustic wave passes through a medium, its amplitude decreases due to attenuation. Attenuation of the wave is caused by adsorption (conversion of acoustic energy into other forms of energy, mainly heat) and scattering. Scattering occurs in heterogeneous media, where the wave is scattered in different directions to the incident wave [45].

First, changes in passive emissions are detected by a sensor. The sensor signal is then usually amplified, and filters are used to remove unwanted frequencies from the signal. The amplified signal is then converted from analogue to digital and visualized using an oscilloscope, spectrum analyzer or PC equipped with the appropriate hardware and software.

Active acoustic systems, instead, typically use specialized devices called transducers to generate and project sonar waves that bounce off objects or marine organisms to measure distance, depth or detect targets. The technology is used in a variety of applications including navigation, fisheries, mapping and submarine detection[46].

4. Image analysis

Image analysis is the general term for procedures and techniques for interpreting and parameterizing information from an image or set of images[47].

The use of image processing in industrial chemical engineering is becoming increasingly common due to advances in imaging technology and the development of several software that works with sophisticated algorithms. On of the main applications of image processing in industrial engineering is process monitoring[48]. Using cameras and image processing algorithms, this technique can be used to monitor in real time the system and potential problems can be identify before they become critical.

The digital image analysis method is a popular, convenient, and effective technique for measuring bubbles size[49]. For many years, researchers have been striving to develop more efficient and precise image processing methods to measure bubble parameters.

The image analysis algorithm involves four main operations[50]:

- Image filtering.
- Separation of the bubbles into solitary and overlapping bubbles.
- Segmentation of the overlapping bubbles using the water shedding technique.
- Combination of the images of the solitary and overlapping bubbles.

Image filtering changes the range (i.e. the pixel values) of an image, so the colors of the image are altered without changing the pixel positions[51], a watershed is a transformation

defined on a greyscale image [52]. The segmented images are used to determine the pixel area of each bubble object. This is then used to determine the average bubble diameter.

5. The importance of controllers in industrial chemistry

Sensors playing an essential role in production for years: in industrial automation, sensors are crucial to making systems intelligent.

A sensor is a device that detects an input stimulus, which can be any quantity, property, or condition of the physical environment, and responds with a measurable digital signal. For instance, the input stimulus can be pressure, force, flow, light, heat, motion, humidity, or any other environmental phenomenon. The output response is usually an electrical signal, such as voltage, current, capacitance, resistance, frequency[53].

A robust sensor is sensitive to the measurand and insensitive to other properties likely to be encountered in its applications[54]. This is referred to as the selectivity of the sensor. A good sensor is also not permanently influenced by the measured property.

5.1 Classification of sensors and their applications

A pressure sensor is a device that measures the pressure of gases, liquids, or solids in terms of mechanical force. Typically functioning as a transducer, it generates a signal based on the applied pressure[55]. Nowadays, pressure sensors are widely used for controlling and monitoring various measurements such as fluid/gas flow, speed, water level, and altitude. They are also known by other names, including pressure transducers, pressure transmitters, pressure senders, pressure indicators, piezometers, and manometers[56]. These sensors are frequently used in the automobile sector, aviation sector, medical sector, computers, cooking appliances, and other daily life applications.

Temperature sensors detect changes in physical parameters, such as resistance or output voltage, which correspond to temperature variations. There are two primary types of temperature sensing[57]:

- **Contact temperature sensing:** This method requires the sensor to be in direct contact with the material or object being measured. It is suitable for monitoring the temperature of solids, liquids, or gases across a very wide temperature range.

- **Non-contact temperature sensing:** This technique involves interpreting the radiant energy emitted by a heat source in the infrared part of the electromagnetic spectrum. It is effective for monitoring non-reflective solids and liquids, but not gases, due to their inherent transparency.

These sensors are used, for example, in the automobile sector, aviation sector, medical sector, computers, cooking appliances, and other daily life applications[58].

Flow controllers are massive flow meters, while their manipulated variable is the percentage of valve opening, which then regulates the flow rate. Flow sensors are used to measure the movement of a fluid over time. A fluid flow can be either a gas flow or a liquid flow. The movement of a fluid can consist of the mass moved, the distance moved, or the volume moved. The flow can then be measured in terms of mass flow (weight per second), average velocity (meters per second) or volumetric flow (volume of fluid per second). In order to measure a flow rate (mass, velocity or volume), a device must translate from the physical domain to the electrical domain. There are several techniques to make the translation from fluid flow to an electrical signal[59]. The technique to be used depends on whether the fluid is a gas or a liquid and the type of flow measurement to be obtained (mass, velocity or volume).

Flow sensors are utilized in numerous fields, such as biomedical applications, environmental monitoring, automotive systems, and process control. In the biomedical field, these sensors are specifically used to measure blood flow within blood vessels[60].

Then there are other controllers that measure other quantities, all with the same aim: to know what is happening in the reactor at any given moment, to ensure that the process is running as desired, to avoid safety problems and to optimize processes.

5.2 Controllers used in the current era

"Industrie 4.0" or the Industrial Internet of Things (IIoT)[61] are terms used to describe the current revolution in industrial automation and control. Everything is becoming smarter, and data generated at all levels of the production process are being utilized to enhance product quality, flexibility, and productivity. This progress is largely driven by smart sensors, which generate crucial data and enable advanced functionalities such as self-monitoring, self-

configuration, and condition monitoring of complex processes. Similar to Industry 4.0, the evolution of sensors has gone through distinct stages, culminating in today's smart sensors, also known as "Sensor 4.0". Efficient data collection technology is critical to a smart factory environment. Intelligent sensors play a key role in the design of IoT technologies for production, by simplifying integration and analysis[62].

A smart choice of sensor, for example, is to build a sensor that fits outside the plant pipe so that it avoids all the problems of being inside: it is no longer invasive; there are no problems of build-up, corrosion or degradation, there is no inconvenience of removing the sensor and if it needs to be done, there is no need to stop production and dismantle the plant.

6. Use of acoustic in the context of chemical engineering

This section gives some examples of the use of passive acoustic systems in industry: there are many areas where this technique is used because it is advantageous.

Acoustic monitoring techniques offer several advantages over optical techniques like near-infrared and Raman spectrometry for process monitoring, especially because they can be used with optically opaque samples without needing any sample preparation. A key benefit of acoustic waves is their ability to penetrate materials such as stainless steel, allowing for non-invasive monitoring. This can be done by attaching sensors or placing a microphone close to the outer vessel wall, avoiding the need for a window in the vessel.

Although the use of non-invasive active acoustic techniques for in situ process monitoring has been reported infrequently, passive acoustics has been more widely adopted, particularly for monitoring particulate processes. Passive acoustic monitoring relies on acoustic emission (AE) generated by particle collisions, primarily with the inner surfaces of vessel or pipe walls, but also with internal structures or between particles. This AE data provides insights into the process status.

Passive acoustic monitoring has been effectively used in various applications, including:

- High-shear granulation[63–66]
- Powder blending[67]
- Drying[68]
- Fluidized bed processes[69–72]

- Heterogeneous reactions[73–77]
- Transport of powders[78,79]
- Transport of tablets[80]
- Transport of slurries[81]

These techniques have demonstrated success in monitoring and providing valuable information about the processes mentioned above.

Another industry that uses the PA system is solid-liquid (S-L) mixing, which is very important in industrial processes such as adsorption, crystallization, leaching and solid catalyst reactions[82]. In industrial processes, stirred tanks are commonly used to improve the interaction between different phases (solid, liquid and/or gas). These tanks are specifically designed to maximize the contact area between phases and to prevent solid particles from settling to the bottom of the tank. The main mechanism to achieve this is the use of an impeller, which generates fluid movement and facilitates the transfer of momentum within the tank[83]. There have been several successful attempts at utilizing AE in order to demonstrate the sensitivity of statistical and spectral features of the signals to variation in the physical characteristics of (S–L mixing), including particle diameter, solid loading and density[84]. Nevertheless, the AE from solid suspension in stirred vessels has only recently been the subject of investigation[85].

Another area in which PA can be applied is in the agricultural sector. This is to control irrigation systems in order to limit water wastage and losses[86]. It can be argued that water constitutes the most precious of all natural resources on the planet, with the potential to become the subject of local conflict across the globe. Indeed, several studies have highlighted the issue of water scarcity and its potential to become a source of tension and conflict between communities and countries[87]. Agriculture is by far the largest sector in water consumption, accounting for 60%–90% of the total water available for human use[88]. Furthermore, the projected increase in population and the effects of climate change will further reduce the availability of this resource. It is therefore essential to devise effective solutions in the field of engineering with a view to limiting losses and detecting faulty water supply systems. This is an initial attempt to integrate a mechanical design, a single passive acoustic emission sensor, and supervised machine learning to identify changes in the fluid (as opposed to the

structure, such as the pipe wall) in order to detect blockages in an unbranched pipe system. The flow field is visualized by utilizing two-dimensional particle image velocimetry (PIV), and the pressure drop is quantified for each obstacle.

Two sensor systems are available for acoustic emission measurements. These sensors can be either active, i.e. based on an emitter-receiver system, or passive. Whereas active acoustic emission sensors measure the change in introduced acoustic waves (sometimes referred to as slot waves) over the distance from the emitter to the receiver, passive acoustic emission sensors only detect the acoustic emission emitted by the process itself[89].

Thus, active acoustic emission is based on an active energy input, whereas passive acoustic emission simply measures the energy output.

7. Use of acoustic emission in combination with machine learning

Machine learning (ML) has the potential to overcome the limitations of mechanistic modelling because ML methods can learn complex behaviors, model development is cheaper, and it can be advantageous for optimization[90]. Today we have cheap and powerful computers, easy-to-use programming environments and a large open-source ML community.

ML is a subclass of Artificial Intelligence (AI). It originated as an application of computer science and mathematics and gives computers the ability to learn from data without being explicitly programmed. ML is broadly divided into supervised learning and unsupervised learning[91]. Other types of ML include reinforcement learning (RL) and hybrids such as semi-supervised learning. The key to machine learning is having a large and high-quality data set in order to build the statistical model.

New deep learning and predictive analytics algorithms hold the potential to greatly accelerate sustainable chemistry design. By using deeper neural networks, which provide a hierarchical representation of the data, deep learning methods have proven to have much more powerful learning capabilities, resulting in higher performance and accuracy in finding new chemical technologies, for example for catalysis. Deep learning techniques can be fed directly with raw data, have automatic features and are able to learn quickly to perform various data processing and predictive analysis tasks efficiently. Many research studies have reported the application to chemical molecular generation and property prediction[92].

Coupling machine learning with multi-channel sound localization systems is emerging as a potential solution[93].

The use of acoustic sensor arrays to provide spatial information in this way not only enables precise localization of sounds but can also be used to improve data quality by removing noise and enhancing signal strength in multiple time-synchronized recordings of a target sound[94].

This involves synchronizing the recordings between different sensors, producing high-dimensional data that can be difficult for observers to visualize or process. Such data could be analyzed by deep learning algorithms to improve the measurement.

Coupling passive acoustic analysis techniques with an automatic data processing and storage system could therefore be a major breakthrough for research in the chemical-industrial field, increasing the speed and allowing much more refined and precise processing.

Materials and methods

The experimental design involves the use of a tubular reactor in which two fluids are mixed that is water and air.

1. Materials

- Water flow dispensed by a pump that works in continuous way.
- Gas flow dispensed by a pump, in particular the gas is air.
- Static mixers made in PLA: polylactic acid resin printed by *Flashforge* 3D printer.
- Acoustic passive sensors (Vallen System).
- Hamamatsu digital camera C8484-05CP.
- Keller pressure measurement device.

2. Methods

The three variables of the system to be analyzed are the gas flow rate, the liquid flow rate and the presence or absence of static mixers, with two configurations. In this way, different fluid dynamic regimes with different conditions can be analyzed.

2.1 Design of the plant

To carry out the tests, a tubular reactor is used in which the gas-liquid flow is co-current, in particular from the bottom to the top. The reactor has a part where mixing takes place using static mixers; they are used to complement or even replace a conventional agitator. Their use in continuous processes is an attractive alternative to conventional agitation as similar and sometimes better performance can be achieved at lower cost. The prototypical design of static mixers is a series of identical, stationary inserts, called elements and their purpose is to redistribute the fluid in a direction transverse to the main flow, which is in the radial and tangential directions. The effectiveness of this redistribution depends on the specific design and number of elements.[95]

The pipe used is 22 mm in diameter and has a section of Plexiglass, so that it is possible to see what is happening inside the tube: in fact, this is the limit of industrial reactors, because it is useful to compare the numerical and computational predictions with the physical

phenomenon. This Plexiglass section is connected to the pipe by means of PLA supports obtained thanks to the 3D printer. Also, the static mixers are made by PLA, in two configurations: clock wise and anticlock wise.

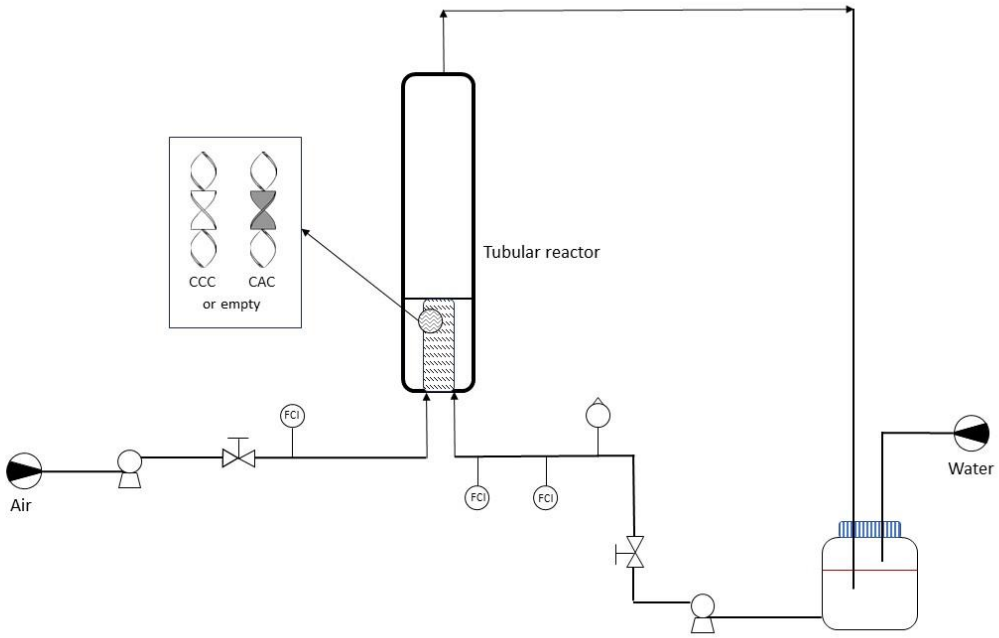

FIGURE 8 - PLANT DIAGRAM

As seen in *Figure 8*, both gas and liquid enter from the bottom of the pipe and exit from the top, driven by two pumps. On the gas side there is one valve and one flow controller, while on the liquid side the control system is duplicated, i.e. there is one valve and one rotameter and two flow controllers. Fluids entering the reactor can find themselves in three different situations: the tube can be empty or filled with static agitators, once with a CAC configuration and then with a CCC. At the reactor outlet, a pipe carries the liquids to the tank. This promotes water recycling.

2.2 Choice of water and air flow rates

Three water and three gas streams were selected, for a total of nine combinations of fluid dynamic regimes. In particular, reference was made by flow pattern map from which you can select the fluid dynamic regime you wish to test (*Figure 9*[96]).

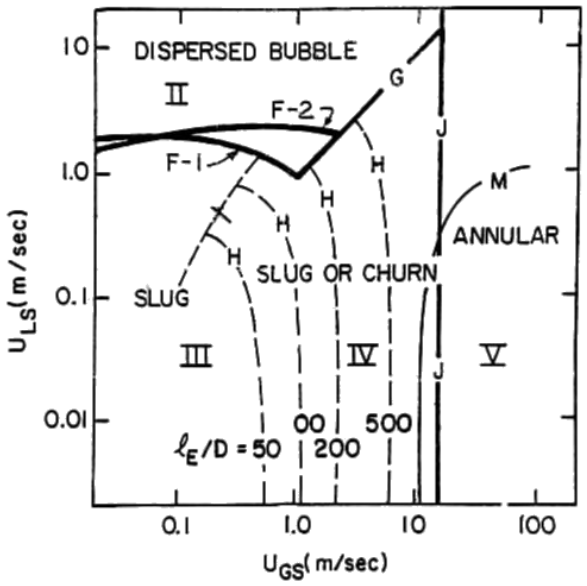

FIGURE 9 – FLOW PATTERN MAP: UPWARD FLOW IN A 2,5 DIA. TUBE. AIR-WATER AT 1.0 ATM

Within the limits of the pump's maximum power, the slug flow and churn flow zones were analyzed as entering the dispersed bubble zone required too high a liquid velocity, while maintaining annular flow needed a very high gas velocity.

Vertical slug flow is characterized by the rise of long, spherical gas bubbles with a diameter close to that of the pipe[97]: these are known as Taylor bubbles, which occupy almost the entire cross-section of the tube.

In churn flow, the large Taylor bubbles characteristic of slug flow have disappeared but, when churn flow is viewed from the outside through a transparent tube, characteristic reversals in flow velocity are observed. It has similarities to annular flow in that there is a continuous gas core in the center of the channel and a layer of near the channel wall; in fact, since 1985 the alternative name "semi-annular" flow has been used. The characteristic that distinguishes it from the annular flow is the breakdown of the slug flow, which is accompanied by a very rapid increase in the pressure gradient due to increased wave activity and friction[98].

In this experiment, the speed of the liquid and the speed of the gas were chosen as follows (*Table 2*):

Liquid speed	Gas speed
0,333 m/s	0,067 m/s
0,689 m/s	0,324 m/s
1,000 m/s	0,864 m/s

TABLE 2: SPEED OF THE LIQUID AND OF THE GAS.

Then the liquid speed is set, the gas speed is changed and so three tests are run for each liquid speed.

Another variable is given by the static mixers, specifically there are three cases:

- Absence of static mixers
- Three static mixers in clockwise mode
- Three static mixers, two in clockwise mode and one in anticlockwise mode, alternately.

So, for all the cases above, measurements were taken for each combination of gas and liquid velocity, as described before.

2.3 Static mixers

Static mixers are used inline in a once-through process or in a recirculation loop where they are an addition to, or even a replacement for, a conventional agitator as similar and sometimes better performance can be achieved at lower cost. Stationary mixers typically have lower energy consumption and reduced maintenance requirements as they have no moving parts[99].

A static mixer is a device consisting of a series of flow directing elements inserted along the axis of the pipe. Pressure drives the fluid through the device, providing the energy required to achieve mixing.

The commercial mixers selected for this study were two types of Kenics static mixers, consisting of a series of mixing elements, each in the shape of a short helix. These mixers were configured in three variations: one with all elements rotating clockwise, and another with elements alternating between two clockwise and one counterclockwise. The elements are arranged in an arc, with each trailing edge perpendicular to its leading edge. The specific geometry of these elements dictates the type of mixing achieved[100]: when all three

components rotate in the same direction, the flow is dispersed, while an alternating orientation concentrates the flow.

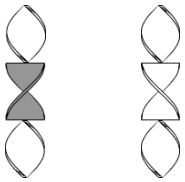

FIGURE 10 - DESIGN OF THE STATIC MIXERS: CAC AND CCC

Mixers are designed using Computer Aided Design (CAD), which is a way of digitally creating 2D drawings and 3D models of real products before they are manufactured, and then obtained thanks to the *Flashforge* 3D printer.

2.4 How an oscilloscope works

An oscilloscope is a measurement tool that provides a graphical representation of a signal's variation over time. It can plot a variety of signals (usually voltage or current, however pressure and vibration sensors are available for automobile oscilloscopes) thanks to probes and sensors linked to its input channels. Oscilloscope displays are always read from left to right. The voltage-time characteristics of the signal, or waveform, is drawn as a line called trace.

The vertical and horizontal scales of the display can be changed on the majority of oscilloscopes. The vertical scale, also known as the input range, is measured in volts in this experiment, but it can be expressed in a number of different units. The horizontal scale is called The horizontal scale is called the collection time and is measured in units of time, in this experiment milliseconds.

2.5 Parameter settings on PicoScope

Prior to initiating the tests, the settings of the industrial reactor prototype must be established using the PicoScope program.

The parameters required are:

- Maximum voltage amplitude [V]: signal values exceeding these limits are stored in the files as ±INF values. This option gives the possibility to select the maximum values, both positive and negative, that the software will accept as real. mat numbers.

While it is not recommended to set values too high as this could result in a loss of signal resolution ±500 mV has been used for all the measurements.

- Buffer number: the sample that will be recorder and stored in the file is called a buffer number and it is saved in the file *.mat* as a vector composed of voltage levels. The buffer, sometimes known as an episodic buffer, is a type of capacity-limited temporary storage that serves as an interface between several systems with various fundamental memory codes. It is believed to be episodic, meaning that it has the capacity to hold episodes-integrated chunks of knowledge that later become conscious awareness.
- Buffer duration [ms]: [2000]
- Number of samples determines the maximum number of samples (MS) that each channel will be able to record. In this experiment, the number of samples chosen is 200 MS.
- Hardware resolution: sets the number of hardware bits used for sampling. In this investigation, it was decided to use 12 bits.
- Collection time: sets the time represented by horizontal axis when the horizontal zoom control is set to x1. In this case it was used 500 μs/div.

Once the set of parameters has been selected, the acquisition can begin.

2.6 Acquisition of noise emission data

Acoustic emission data were collected using a piezoelectric sensor placed on the outer wall of the reactor. In particular, two passive acoustic emission sensors are used and it was designed to record data in two zones: before and after mixing, which is done by the static mixers. This choice was made because we want to verify how the sensor perceives and sees the effects of mixing.

The preamplifier first processed the signal from the sensor, which was generated by vibrations in the reactor by water jet, amplifying in the acoustic signal. The amplifier in the decoupling box then decoupled the amplified signal.

Ultimately, an oscilloscope was used to process the acoustic emission data; Picoscope 6 software was used to record and display the time signal on the PC screen. Both the. mat and *.psdata* formats were used to store data.

2.7 Data analysis using MATLAB

Once all data has been saved in. mat format, it is processed using the MATLAB software.

The experiment to be analyzed is chosen, and the folder containing the files related to the measurements of that experiment is then opened.

```
T = 1.336*10^(-6);    % sampling period
Fs = 1/T;    % sampling frequency

L = 2000000;    % length of signal
t = (0:L-1)*T;    % time vector

syst=942;
id1=17;
id2=71;
pipe="CCC";

Ptot=zeros(25,1000001);
Atot=zeros(1,1000001);
for i=1:25
    if i<10
        filename=strcat('C:/Users/lisad/OneDrive - Alma Mater Studiorum Università di Bologna\waveforms/CCC/L',num2
        load(filename);
    elseif(i>11)
        filename=strcat('C:/Users/lisad/OneDrive - Alma Mater Studiorum Università di Bologna\waveforms/CCC/L',num2
load(filename);

    end

    Y=fft(A);
    P2 = abs (Y/L);
    P=P2(1:L/2+1);
    P(2:end-1) = 2*P(2:end-1);
    f = Fs*(0:(L/2))/L;
    Ptot(i,:)=P;

end

Pfinal942CCC=sum(Ptot);
```

FIGURE 11 – MATLAB SCRIPT

The “open(filename)” function in MATLAB loads and opens all files.

The Fourier transform (fft) is here used to convert the time domain, the unit in which Picoscope data is stored, to frequency. In mathematical analysis, Fourier analysis is a branch of research that stems from the work of Jean-Baptiste Joseph Fourier, who in the early 19th century was able to prove that every continuous function can be seen as a sum of appropriate sinusoidal functions. Thanks to this discovery, it was possible to decompose complicated functions into a series of functions, known as Fourier series, which make their analysis easier. This is also known as harmonic analysis[101].

In MATLAB, the syntax Ptot(i,:) = P; is used to assign values to a particular row of a matrix Ptot. Here's a breakdown of what this line of code does:

- Ptot is a matrix or 2D array.
- i is the index of the row in the matrix Ptot that you want to change.
- The colon : operator indicates that you want to select all columns in the i-th row.
- P is a vector (row vector) whose values you want to assign to the ith row of Ptot.

Pre-allocating Ptot can improve your MATLAB code, especially when working with large matrices or looping. Ptot is 25x1000001 matrix and the final output is plotting the total sum of Ptot.

A total of 25 tests were conducted and what is observed at the conclusion is a two-dimensional graph depicting intensity versus time (*Figure 12*).

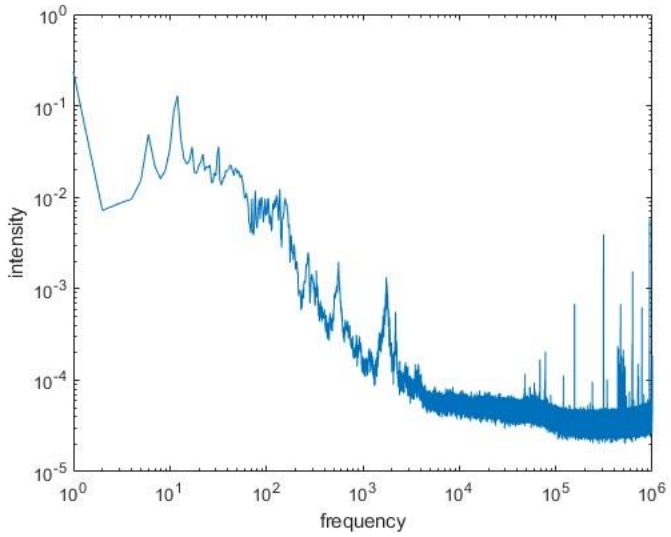

FIGURE 12 – LOGLOG OF INTENSITY VS FREQUENCY

In the *Figure 12* is show how the intensity changes in the course of time: these intensity is given by what the sensor detect.

There is an interest in observing how the intensity values change at different flow rates, and to achieve this, the MATLAB 'Hold on' function is utilized. Hold on keeps the graphs on the axes created for the first plot, so that new graphs added to the axes do not delete exiting ones. New graphs use different colors to distinguish them. MATLAB adjust axis boundaries, tick marks and tick labels to display the full range of data. If the axes do not exist, the hold command creates them[102].

Here is an example of graph generated by a hold on is shown in *Figure 13*: three curves are show in three different colors, and although the trend over time shows a fairly similar profile for all three curves, there are big differences in terms of intensity. Specifically, the graph relates the profiles recorded with a fixed liquid flow rate and a varying gas flow rate.

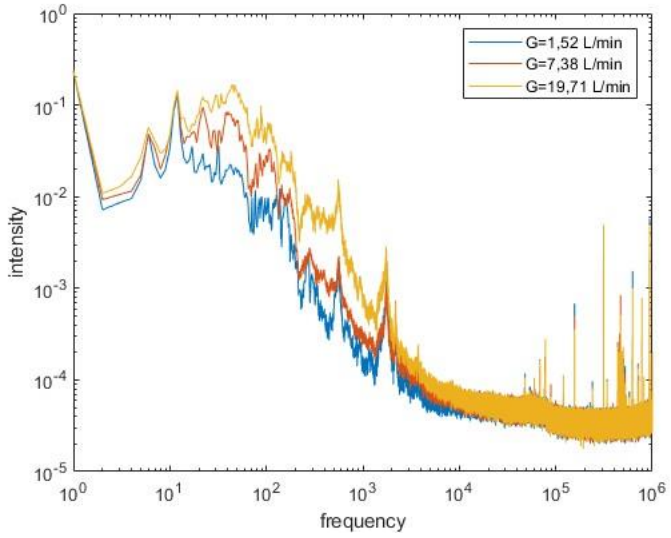

FIGURE 13 – HOLD ON OF THE CURVES OF THREE FIXED GAS FLOW RATES, WITH CONSTANT LIQUID FLOW RATE

The liquid flow rate used in the analysis of the example given is 942,88 L/h, the blue curve corresponds to the gas flow rate equal to 1,51 L/min, the red one is 7,38 L/min and the yellow one is 19,71 L/min.

2.8 Image acquisition and analysis by DynamicStudio

DynamicStudio is the main software package for image acquisition and analysis in for particle sizing areas. It contains tools for configuration, acquisition, analysis, post-processing of acquired data[103]:

- The acquisition system includes auto-detection of devices, cable connection diagrams and supports distributed acquisition over networks.
- The innovative and secure ensemble database gives a simple intuitive display of large amounts of data.
- The built-in presentation and analysis modules give you several possibilities and combinations of processing and display of data.

After creating a database with the name of configuration being analyzed, three parameters were set:

- Time between pulses, which is the time between the two acquisition required to obtain each image pair for cross-correlation. In this case it is 2 seconds.
- Trigger rate, which is the acquisition frequency and here is 10 Hz.
- Number of imagines, which is the number of images to be recorded in the measurement and in this experiment is 2000.
- Exposure time, that in photography is identified as that situation in which the shutter remains open to allow light to enter the sensor, and in this experiment is 468,59 nanoseconds.

During the *preview mode*, all devices synchronize, with the laser flashing as the trigger for the camera to capture images at the specified rate in the system control panel. Image acquisition does not stop after reaching the required number, but continues, overwriting the oldest image with the latest one. The process persists until manually stopped, with the last acquired images retained in the buffer for potential evaluation and storage. This phase is important to ensure that all cameras are positioned correctly and that the focal aperture is optimal for the proper functioning of the system.

So the image acquisition proceeds.

In order to verify that the system is in a steady state for a given measurement under certain conditions, acquisitions were made by recording different numbers of images, namely 100, 200, 500, 1000 and finally 2000, keeping all other parameters the same.

It was checked that from 500 images onwards the power was the same, thus verifying that the system was in a steady state. For a point analysis, 2000 images were therefore chosen to be processed.

2.9 Study of images by grayscale

One of the post-processing methods that can be used with DynamicStudio software is the use of greyscale and consists of the 'raw' measurement for all pixels.

The analysis process typically involves several 4 steps:

- Image pre-processing: Images can be pre-processed to improve quality or to apply specific filters, such as noise reduction or contrast enhancement.
- Feature extraction: salient features are extracted from regions of interest. These can be textures, shapes or other properties specific to the object of interest.
- Quantitative analysis: Extracted features are analyzed quantitatively to extract useful information. This could include calculating statistics such as mean, standard deviation, pixel intensity distribution, etc.
- Visualization and interpretation: Finally, the results of the analysis are visualized and interpreted to provide meaningful information about the object of study. This can be done through graphs, heat maps, or simply by observing the detected features.

In short, the analysis of a set of greyscale images involves manipulating and interpreting the shades of grey to obtain information about the features and content of the images.

The graph (in *Figure 14*) shows the "quantity" of bubbles passing through that specific section under fixed conditions and the aim is to correlate the information from the images with the signals from the passive acoustic sensor.

The data processing steps consist in converting the data from (.cvc) to (.xlsl), from here it is possible to graph the grey intensity percentage values, values acquired as a function of time: if the grey intensity is higher, it means that the sensor is affected by the passage of an air bubble at that moment.

With the usual aim of comparing the different conditions, the same graph show the grey intensity trends at constant liquid flow rate and the same static mixers, but with different gas flow rates.

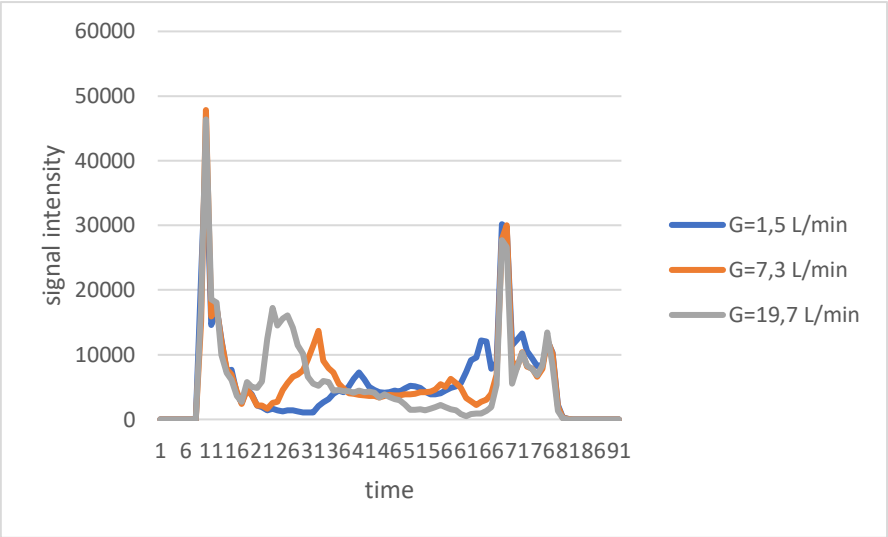

FIGURE 14 – GREY SCALE VALUES

2.10 Correlating passive acoustic analysis and imaging

The analysis of the signals recorded by the passive acoustics was carried out using MATLAB. The loading of the data is by means of the same commands as in the script in *Figure 10*, but a filter is added. In MATLAB, a high-pass filter is a type of filter that allows the high-frequency components of a signal to pass through while attenuating (reducing) the low-frequency components. This type of filter is often used in signal processing to eliminate low-frequency noise or to extract the high-frequency components of a signal.

```
load(filename);

    end

Ahigh=highpass(A,4000,Fs);

if(i==1) Atot=Ahigh;
else Atot=Atot + Ahigh;
end

    Y=fft(Ahigh);
    P2 = abs (Y/L);
    P=P2(1:L/2+1);
    P(2:end-1) = 2*P(2:end-1);
    f = Fs*(0:(L/2))/L;
    Ptot(i,:)=P;

end

Pfinal942CCC=sum(Ptot);
```

FIGURE 15 - MATLAB SCRIPT USING THE FILTER

To continue the analysis, a Matlab application called Signal Analyzer was used to observe the Ptot plots, with the option of superimposing the plots to compare different situations under different conditions.

The results were compared for 3 case studies:

- Same liquid flow, same static mixers and different gas flow.
- Same liquid flow rate, same gas flow rate and different static mixers.
- Same gas flow rate, same static mixers and different liquid flow rate.

The decision to compare these three parameters was taken because the aim is to associate the different signals with the phenomenon that generates them, i.e. whether they are made by the passage of liquid, gas or the system, hence the presence and type of static mixers and everything else about the system.

2.11 Viewing captured images

The analysis of each test was carried out by combining the intensity analysis of the signals recorded with the PA technique with the images taken under the same conditions.

What the camera makes visible is the passage of bubbles of different diameters and with different amounts of intensity.

The camera was fixed in a specific position in order to keep the system as fixed and unambiguous as possible, and visualized the inside of the tube by means of a Plexiglas section.

Each measurement is based on the acquisition of 2000 images: some images are shown below to illustrate the visualization of the bubbles. In the next chapter, we'll look more closely at the analysis, but for now it's enough to say that visualizing the images allows us to distinguish different regimes depending on the case.

The example shown in the *Figure 16* corresponds to experiments carried out at L=455 L/h , G=1,52 L/min , and with filling the tube once empty, then with static mixers CAC and finally CCC.

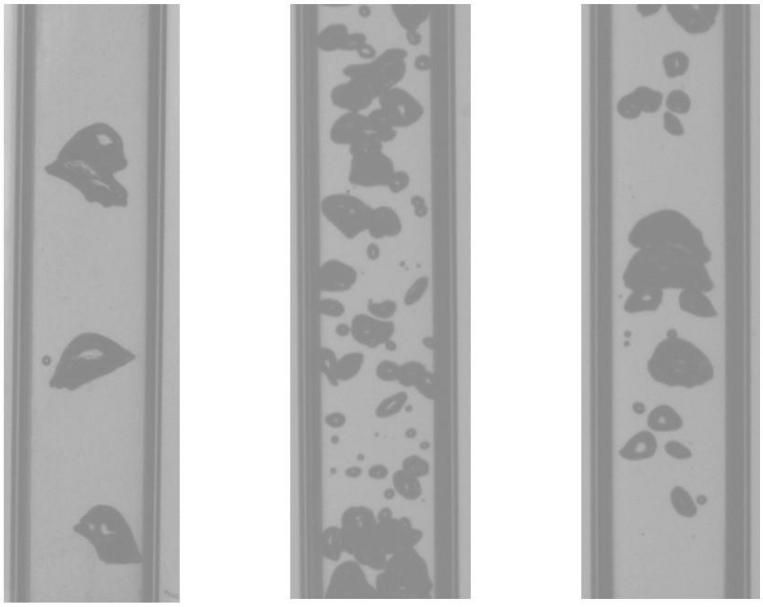

FIGURE 16 - IMAGES FOR WITH L=455 L/H , G=1,52 L/MIN , FROM LEFT TO RIGHT, EMPTY PIPE, CAC, CCC

2.12 Head losses calculation

Pressure drops (ΔP) are the proportion of potential energy lost by the fluid (converted to heat) to overcome the friction it encounters as it flows through a pipe. They depend on:

- The roughness of the inner surface of the tubes.
- The viscosity of the fluid.
- The velocity of the fluid.
- The geometric dimensions of the pipe.

Two main types of head loss can be distinguished.

Distributed head losses occur along the entire length of the pipe and are mainly caused by friction between the fluid and the inner pipe walls. Distributed head losses depend on the length of the pipe, its diameter, the flow velocity, the internal roughness of the pipe and the physical properties of the fluid, such as viscosity. The equation is generally used for calculation, together with the determination of the friction factor, which can vary depending on the flow regime (laminar or turbulent).

$$\Delta P_d = 4f \frac{\rho L}{D} V^2$$

Where:

f is the friction factor;

L and D are the length and diameter of the pipe (m) respectively;

v is the fluid velocity (m/s);

ρ is the density of the fluid (Kg/m^3).

Dimensional analysis shows that pressure is in Pa.

Concentrated or localized pressure drops occur at specific points in pipelines due to the presence of certain components such as valves, bends, fittings, expansions or constrictions. They are therefore independent of the length of the pipe and are associated with changes in fluid direction or velocity that cause turbulence and additional flow resistance.

They are calculated using component-specific loss coefficients that take into account the amount of disturbance that each element introduces into the fluid flow. At these points, the fluid undergoes an abrupt change in direction and velocity due to friction and turbulence: this results in the conversion of pressure energy into heat energy, leading to a significant increase in temperature.

This can be calculated using the following formula:

$$\Delta P_c = \frac{K}{2g} V^2$$

Where:

K is localized coefficient of resistance and it is experimentally determined;

v is its velocity before deflection or throttling (m/s);

g is gravity acceleration.

The flow is due to a pressure difference that pushes the fluid from upstream to downstream. The force F associated with the movement of the fluid can be defined as the total pressure drop multiplied by the fluid flow section:

$$F = |\Delta P| \pi R^2$$

Equivalently, F can be expressed as the product of the wetted surface area A, the kinetic energy per unit volume k and the dimensionless friction coefficient f:

$$F = fAk$$

By combining the two expressions, it is possible to define the friction factor, which is dimensionless and equal to:

$$f = \frac{R}{L}\frac{|\Delta P|}{\rho v 2} = \frac{D}{2L}\frac{|\Delta P|}{\rho v 2}$$

The friction factor represents the total momentum transported (turbulent+laminar) divided by the momentum transported per turbulent mechanism.

We specify the friction factor as a function of average speed *v*:

In the case of laminar motion, the pressure losses are described by the Hagen-Poiseuille:

$$v = \frac{vmax}{2} = \frac{|\Delta P| D2}{32\mu L}$$

Replacing the value of |ΔP| into the friction factor the result obtained is:

$$f = \frac{16\mu}{Dv\rho} = \frac{16}{Re}$$

So there is an inverse proportional relationship between Re and f.

For turbulent flow, on the other hand, various relationships are proposed in the literature, including:

- $f = 0{,}0791/Re^{0,25}$
- $f = 0{,}046/Re^{0,2}$

The values of the friction factor as a function of the Reynolds number are tabulated. This function is represented graphically by means of a diagram, plotted on a "Moody's" plane (*Figure 17*).

The diagram, which is made on a double logarithmic scale, shows the Reynolds number in the abscissa and the friction factor in the ordinate.

In the general case, the diagram is divided into three distinct zones.

The first zone is characterized by the laminar regime and extends up to Re = 2300. In this region, the curve is a straight line with a negative slope.

The second zone is the transition zone: here the diagram is not drawn because its course is unknown.

The third zone, which starts at Re = 4000 - 4100, is characterized by the turbulent regime. In this case the curve starts at a high friction factor value and decreases. If the pipe is smooth, the curve decreases indefinitely; if, on the other hand, the pipe has a certain roughness, the curve assumes a course similar to that of a straight line parallel to the x-axis at a certain Reynolds number.

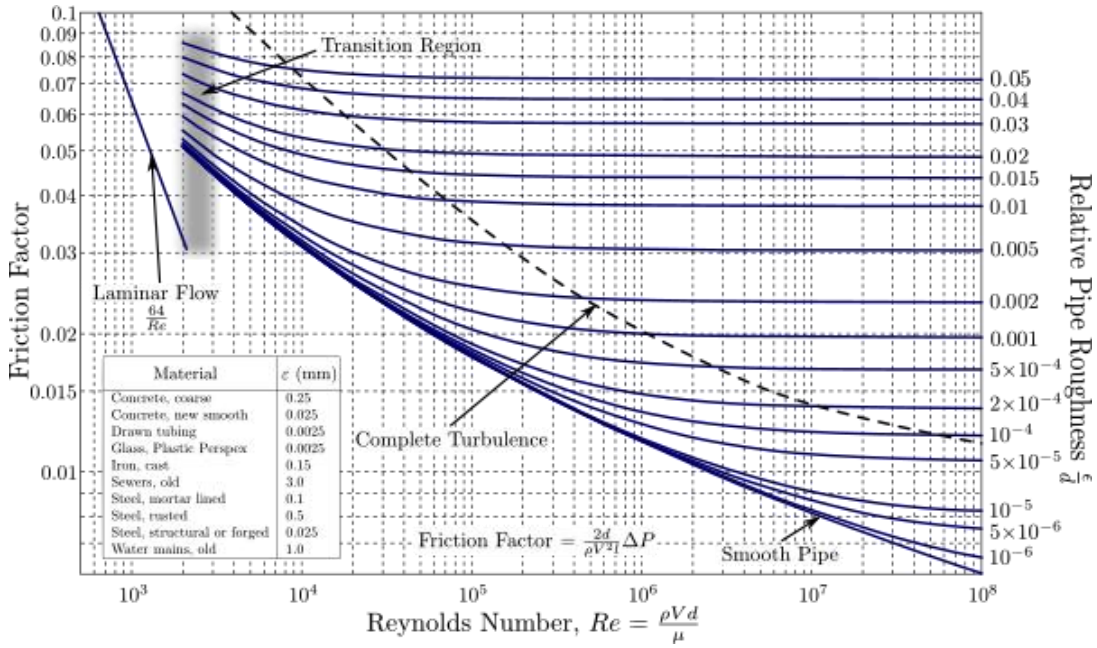

Material	ε (mm)
Concrete, coarse	0.25
Concrete, new smooth	0.025
Drawn tubing	0.0025
Glass, Plastic Perspex	0.0025
Iron, cast	0.15
Sewers, old	3.0
Steel, mortar lined	0.1
Steel, rusted	0.5
Steel, structural or forged	0.025
Water mains, old	1.0

FIGURE 17 - MOODY DIAGRAM

Based on the number of Raynolds, which can be calculated with:

$$\mathrm{Re} = \frac{\rho D v}{\mu}$$

the friction factor is derived.

2.13 Recording of pression drop

The analysis for measuring pressure losses is conducted by measuring the pressure at two different heights of the pipe. This is accomplished using a tool called ControlCenterSeries30 (CCS30), a Windows software which communicates with KELLER instruments connected

to the PC via an interface converter. The computer program displays current pressure values and trend curves, records measurements and exports them as CSV files. The measuring interval can be specified in milliseconds, seconds, minutes or hours. The measurement data is always measured and stored in bar, but it is possible to change the display to another unit.

When the software is opened, it is configured to find the zero point. This is the point at which the instrument is zeroed prior to analysis.

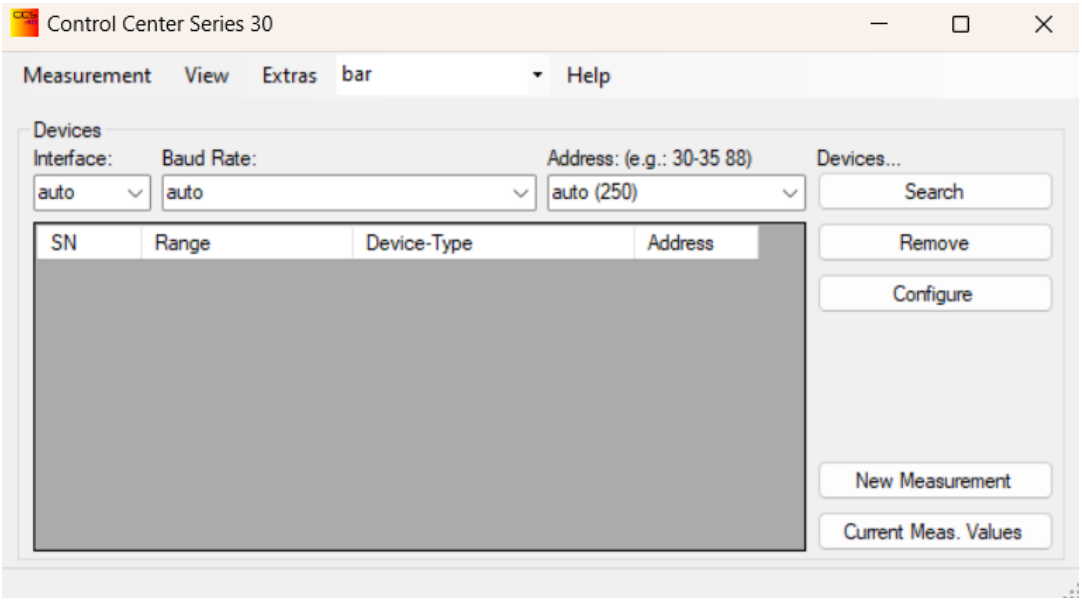

FIGURE 18 - CCS30 SOFTWARE OPENING WINDOW

Then measure the pressure difference by fixing two points on the pipe. Analyses were carried out by fixing the liquid flow rate and increasing the gas flow rate. The flow rates are the same as for the other analyses, as shown in *Table 1*. In the same experiment, therefore, with a constant liquid flow rate, the different pressure drops are visualized: as the gas flow rate increases, the total pressure drops.

Instrument records pressure values in bar. The collected data is then loaded into MATLAB for processing. *Figure 19* shows the plot of the pressure drop recording.

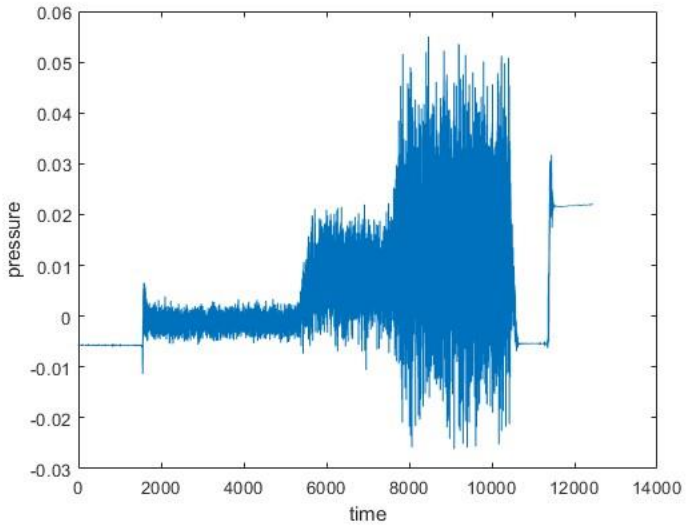

FIGURE 19 – PRESSURE GRAPH AS A FUNCTION OF TIME

There are five different situations that can be identified in the spectrum: they are associated with the flow of water and air.

More specifically:

- from 0 to 1600 is water-only flow
- from 1600 to 5300 is water and first air flow
- from 5300 to 7600 is water and second air flow
- from 7600 to 10100 is water and third air flow
- from 11000 to 12500 is the signal about the pipe full of liquid but at rest.

The last interval will be used as the zero point, this means that for each signal recorded under a given condition, the pressure drop is always the pressure difference between the zero point and the interval of the individual measurement.

In MATLAB, after specifying the intervals, we proceed with the numerical calculation of the pressure drop, as can be seen in the *Figure 20*.

The trend is that as the pressure drop increases, the losses decrease relative to zero.

```
a2=L45575lhCAC(29:1548);
b2=L45575lhCAC(1634:5291);
c2=L45575lhCAC(5468:7513);
d2=L45575lhCAC(7814:10374);
e2=L45575lhCAC(11615:12335);

mediaa1=mean(a2);
mediab1=mean(b2);
mediac1=mean(c2);
mediad1=mean(d2);
mediae1=mean(e2);

devsta1=std(a2);
devstb1=std(b2);
devstc1=std(c2);
devstd1=std(d2);

perdita1=mediae1-mediaa1;
perdita2=mediae1-mediab1;
perdita3=mediae1-mediac1;
perdita4=mediae1-mediad1;

deltaG1=mediab1-mediaa1;
deltaG2=mediac1-mediaa1;
deltaG3=mediad1-mediaa1;
```

FIGURE 20 - MATLAB SCRIPT

The pressure value of each interval is an average of its different values, in fact the "mean" function is used. Once the averages have been calculated, a simple difference to the zero point remains.

Results and Discussion

All tests were carried out using the same procedure, differing only in the combinations of gas or liquid flow rate and the presence or absence of static stirrers.

Once the pump has been switched on, the conditions have been imported and the system monitored by the controllers, we allow the system to run for a few minutes before starting to collect data to ensure that we have reached steady state, i.e. the point from which the variables defining the system remain constant.

The post-processing of the data was carried out using a constant methodology: comparing equal situations with less than one condition.

By working in this way, it is possible to assess, firstly, whether there are differences in the output of the system when a variable is changed, but also which condition has the greatest impact.

1. Characterization acoustic passive results

All the data stored in Picoscope was analyzed using MATLAB software.

1.1 Analysis with different static mixers

Below are the results of the tests carried out with a liquid flow rate of L=455 L/h and the same gas flow rate G=1,52 L/min and with the three different conditions due to the static mixers.

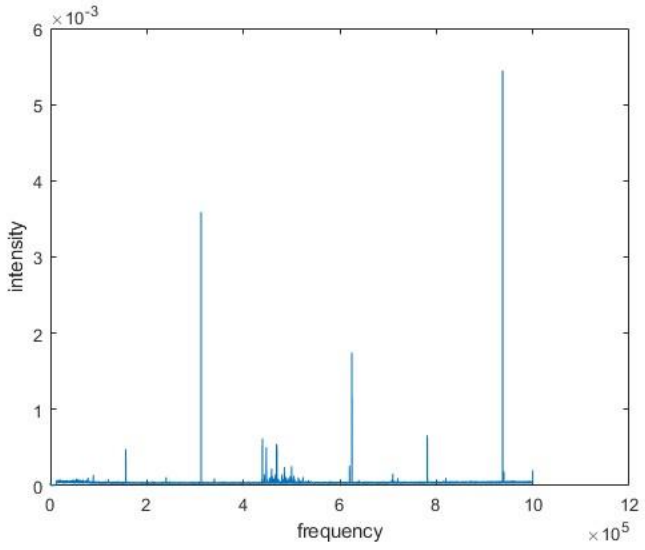

FIGURE 21 - PLOT OF INTENSITY VS FREQUENCY FOR L=455 L/H, G=1,52 L/MIN AND WITHOUT STATIC MIXERS

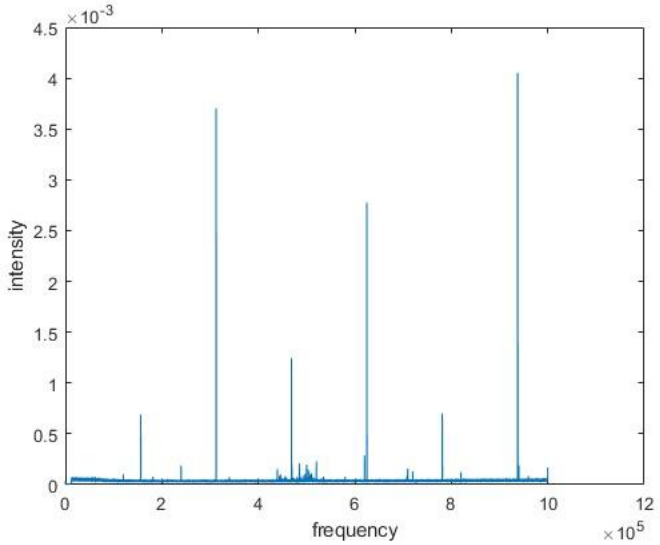

FIGURE 22 - PLOT OF INTENSITY VS FREQUENCY FOR L=455 L/H, G=1,52 L/MIN AND WITH CAC STATIC MIXERS

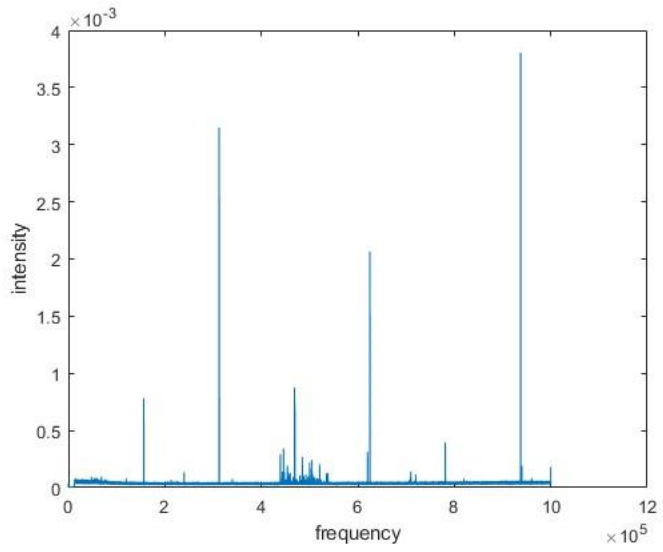

FIGURE 23 - PLOT OF INTENSITY VS FREQUENCY FOR L=455 L/H, G=1,52 L/MIN AND WITH CCC STATIC MIXERS

In *Figures 21, 22, 23* it can be seen that the range between 0 and 4 $x10^5$ and from 6 $x10^5$ to 10 $x10^5$ is constant, it means that the peaks are exactly the same, i.e. at the same frequency value, and have only small differences in intensity. It has therefore been assumed that these are the signals relative to the system, whose intensity varies because the intensity of the phenomenon generating them varies.

In the plots shown in *Figures 21, 22, 23*, three zones can be distinguished: one from 0 to $4.00e^{+5}$ and one from $6.50e^{+5}$ to $1.00e^{+6}$ which are always the same, i.e. they have the same frequency peaks, with only a difference in intensity. This can probably be related to the vibrations of the system, which do not change. Then there is a central zone, from $4.00e^{+5}$ to $6.50e^{+6}$ called the fingerprint, which instead shows peaks at different frequencies, so it is assumed that these are the signals related to the system variables (*Figure 24*).

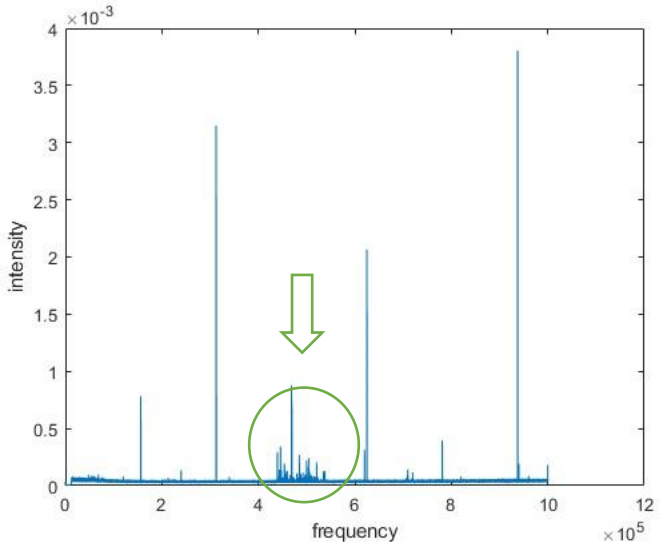

FIGURE 24 - FINGER PRINT OF PLOT

1.2 Analysis with different gas flow rate

Figures 25 and *26* show the graphs for experiments carried out with a liquid flow rate of L=455 L/h and with static mixers of type CAC. What changes is the gas flow rate, which is respectively G_2=7,38 L/min and G_3=19,71 L/min.

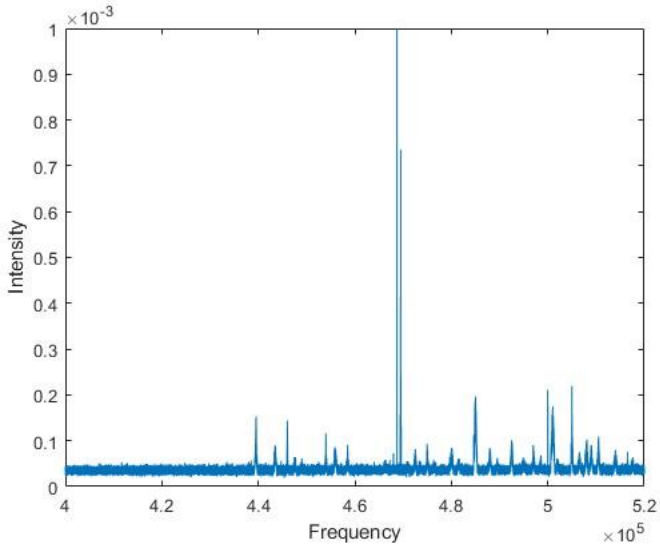

FIGURE 25 – PLOT OF INTENSITY VS FREQUENCY FOR L=455 L/H, G=7,38 L/MIN AND WITH CAC STATIC MIXERS

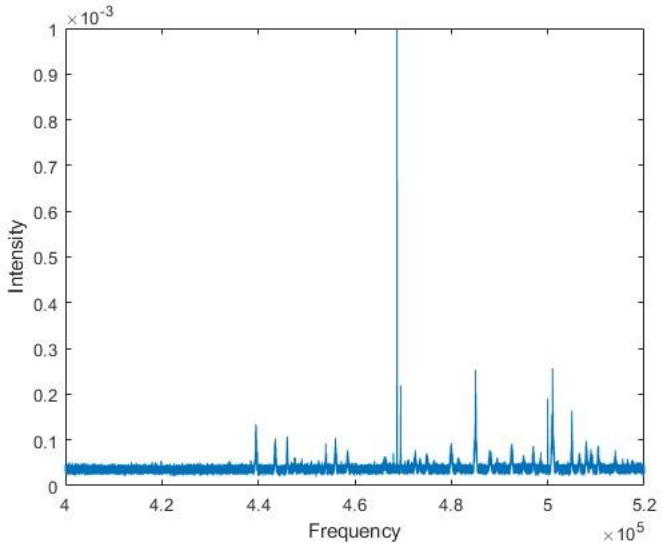

FIGURE 26 - PLOT OF INTENSITY VS FREQUENCY FOR L=455 L/H, G=19,71 L/MIN AND WITH CAC STATIC MIXERS

Under the same conditions of static mixers and liquid flow rate, but with a different gas flow rate, different intensity vs. frequency spectra is still obtained. The observation of the two constant side zones in terms of frequencies remains valid, so here too, only the central zone, i.e., the fingerprint, is evaluated. *Figure 22* is also taken into account.

1.3 Analysis with different liquid flow rate

Below are graphs of tests with the same conditions in terms of gas flow rate and static mixers, i.e. G=1,52 L/min and CAC mixer, and different liquid flow rate. In detail, *Figure 27* refers to the water flow rate of L_2=942 L/h and *Figure 28* is about L_3=1368 L/h. *Figure 22* is also taken into account.

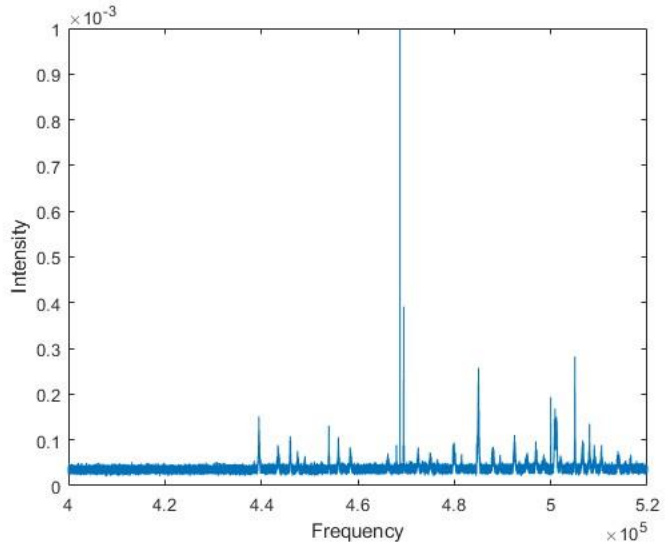

FIGURE 27 - PLOT OF INTENSITY VS FREQUENCY FOR L_2=942 L/H, G=1,52 L/MIN AND WITH CAC STATIC MIXERS

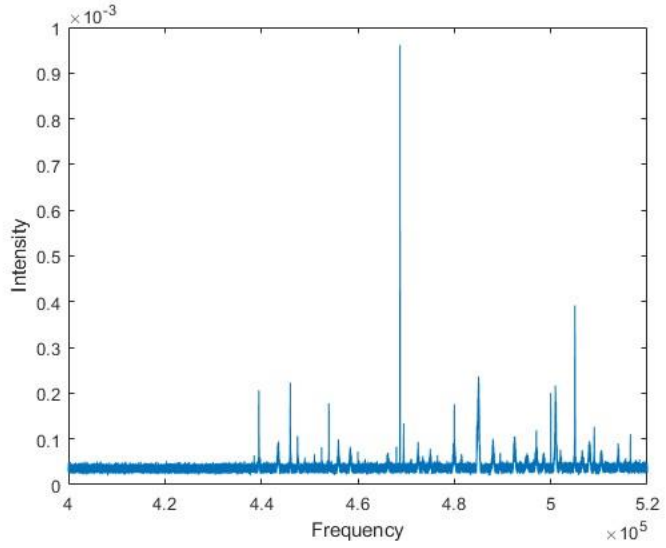

FIGURE 28 - PLOT OF INTENSITY VS FREQUENCY FOR L_3=1368 L/H, G=1,52 L/MIN AND WITH CAC STATIC MIXERS

The area of interest is again the central one, formerly called finger print, where differences are noticeable.

2 Comparison passive acoustic with images

To understand what is happening inside the tube and what causes the differences in the signals in the passive acoustic spectra, the images taken by the camera are shown.

Three different cases are shown: *Table 3* contains the system conditions for the cases considered.

Figure	Liquid flow	Gas flow	Pipe filling
Figure 9	L=455 L/h	G=1,52 L/min	Empty pipe
Figure 10	L=942 L/h	G=7,38 L/min	CAC
Figure 9	L=942 L/h	G=7,38 L/min	CCC

TABLE 3 – PARAMETERS ASSUMED IN EXPERIMENTS.

How different physical phenomena produce different signals can be seen visually by plotting the PA signals alongside the bubble images.

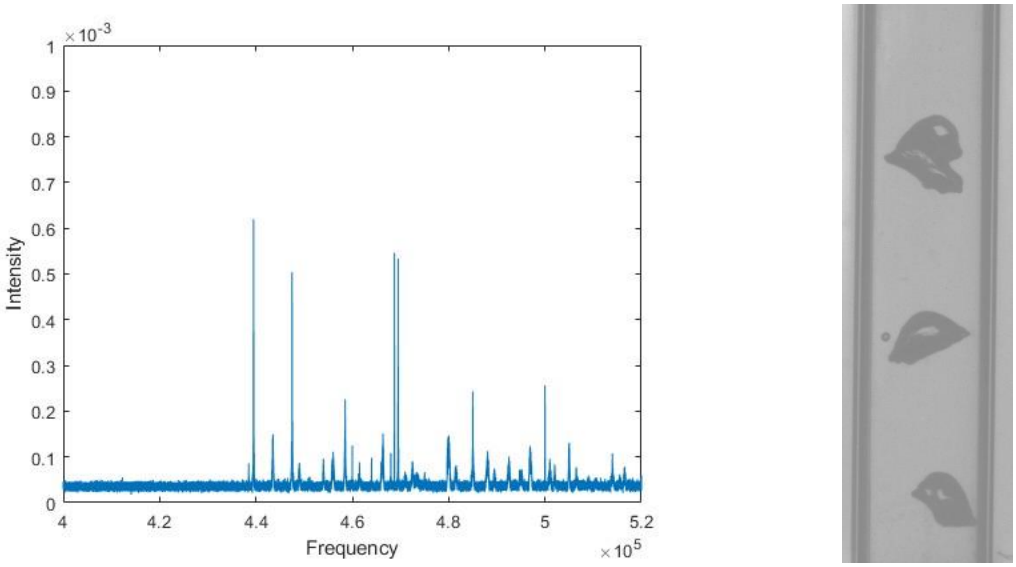

FIGURE 29 - ON THE LEFT, PLOT OF INTENSITY VS. FREQUENCY FOR L=455 L/H, G=1.52 L/MIN AND WITHOUT MIXERS, ON THE RIGHT, PICTURE OF THE PIPE UNDER THE SAME CONDITIONS.

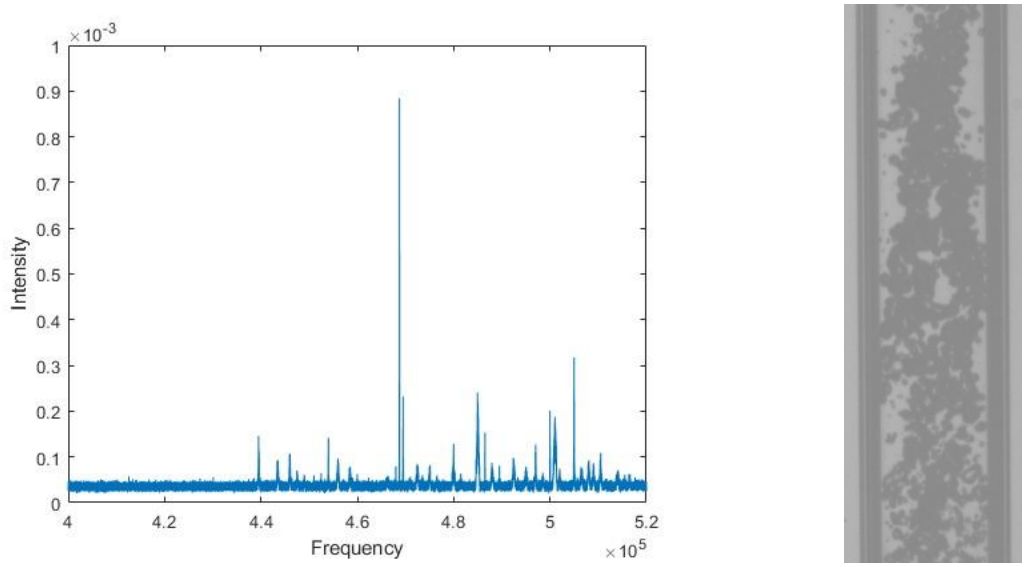

FIGURE 30 - ON THE LEFT, PLOT OF INTENSITY VS. FREQUENCY FOR L=942 L/H, G=7,38 L/MIN AND WITH CAC MIXERS, ON THE RIGHT, PICTURE OF THE PIPE UNDER THE SAME CONDITIONS.

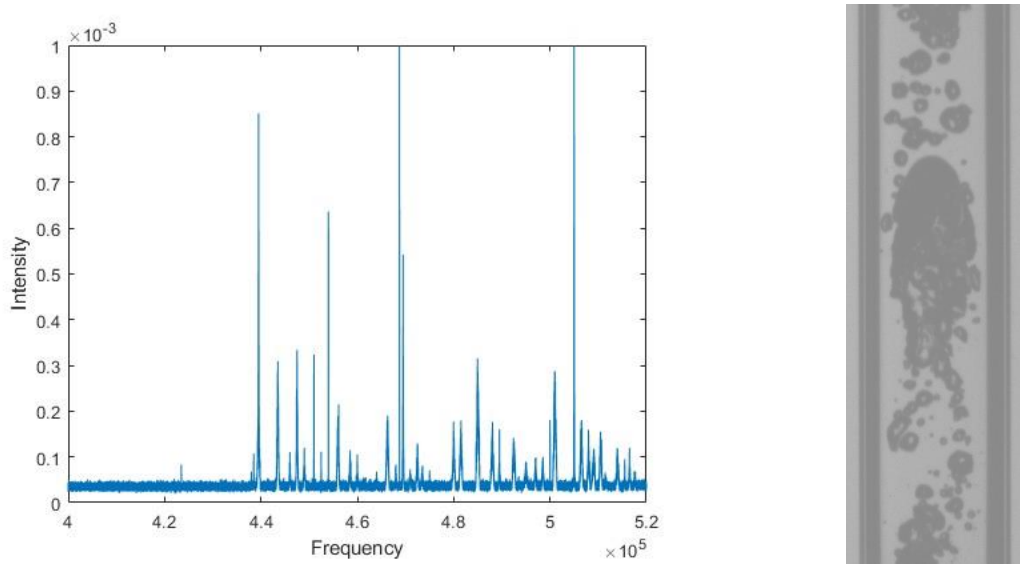

FIGURE 31 - ON THE LEFT, PLOT OF INTENSITY VS. FREQUENCY FOR L=942 L/H, G=7,38 L/MIN AND WITH CCC MIXERS, ON THE RIGHT, PICTURE OF THE PIPE UNDER THE SAME CONDITIONS.

One way of better observing and verifying signal differences in different cases is to use ***hold on***, a feature of the Matlab software that keeps plots on the current axes so that new plots added to the axes do not delete existing ones.

2.1 Comparison of images

Images are a useful tool for comparison. Examining the actual situation reveals that the phenomenon varies in each instance. The images for all parameter combinations are presented below.

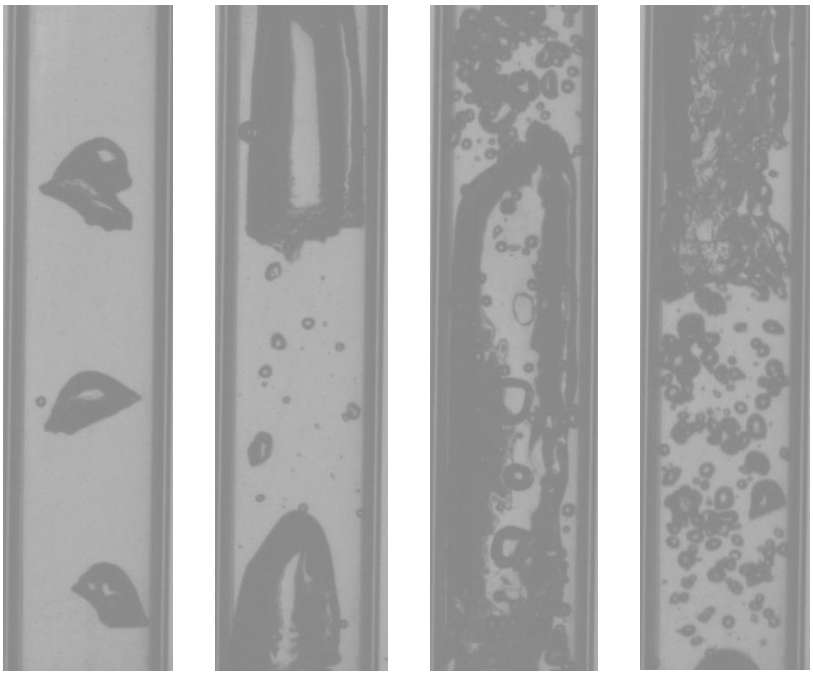

FIGURE 32 – L=455 L/H, EMPTY PIPE, IN ORDER LEFT TO RIGHT, G_1=1,52 L/MIN, G_2=7,38 L/MIN, G_3=19,71 L/MIN, BUBBLE ENTRAINMENT AREA WITH G_3.

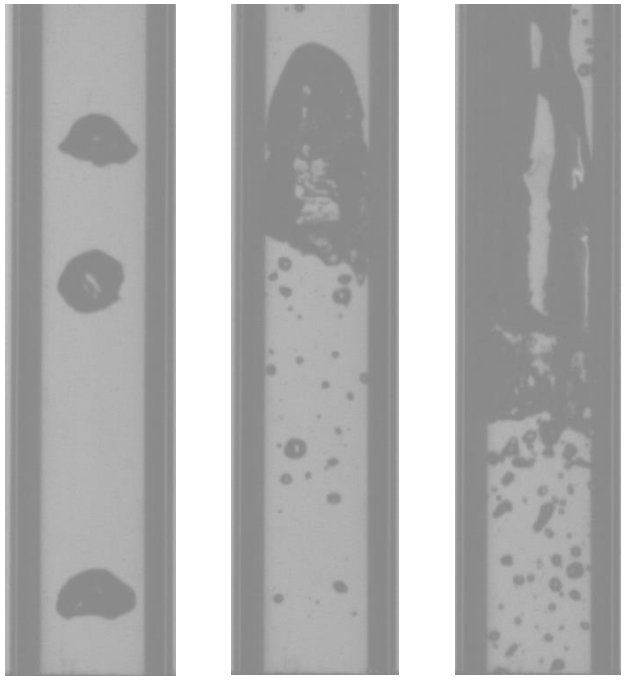

FIGURE 33 - L=942 L/H, EMPTY PIPE, IN ORDER LEFT TO RIGHT, G_1=1,52 L/MIN, G_2=7,38 L/MIN, G_3=19,71 L/MIN.

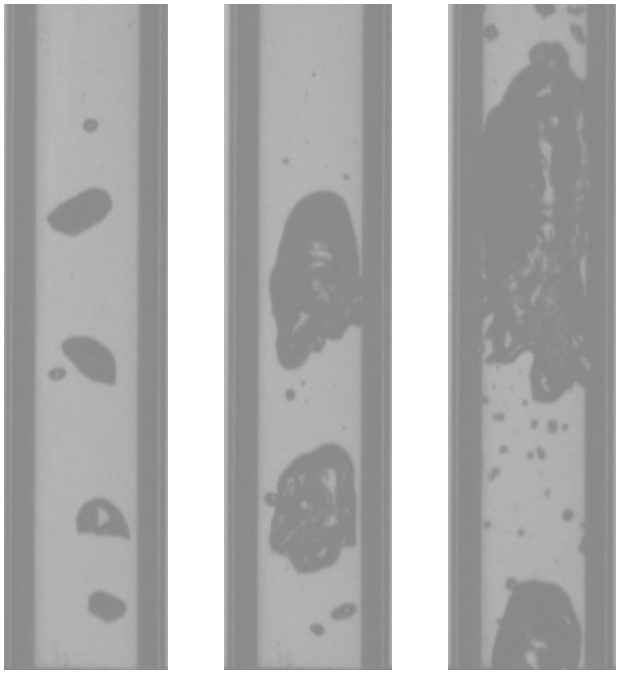

FIGURE 34 - L=1368 L/H, EMPTY PIPE, IN ORDER LEFT TO RIGHT, G_1=1,52 L/MIN, G_2=7,38 L/MIN, G_3=19,71 L/MIN.

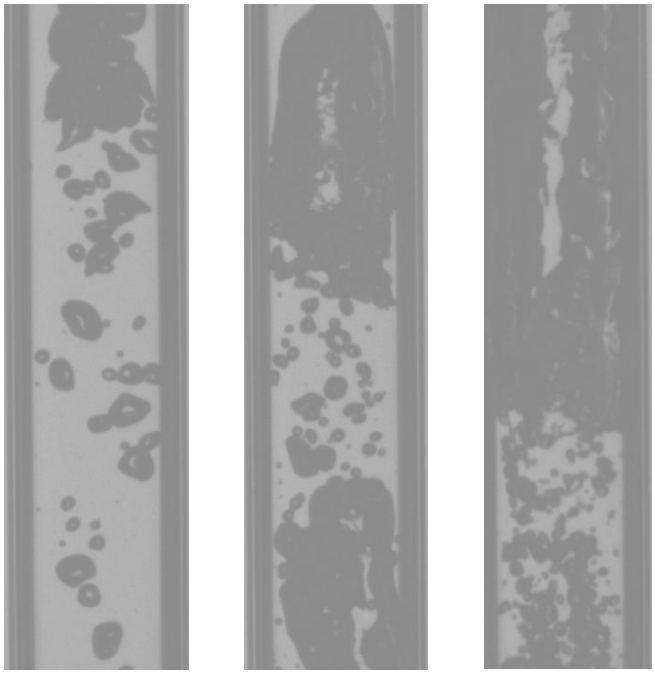

FIGURE 35 - L=455 L/H, CAC, IN ORDER LEFT TO RIGHT, G_1=1,52 L/MIN, G_2=7,38 L/MIN, G_3=19,71 L/MIN.

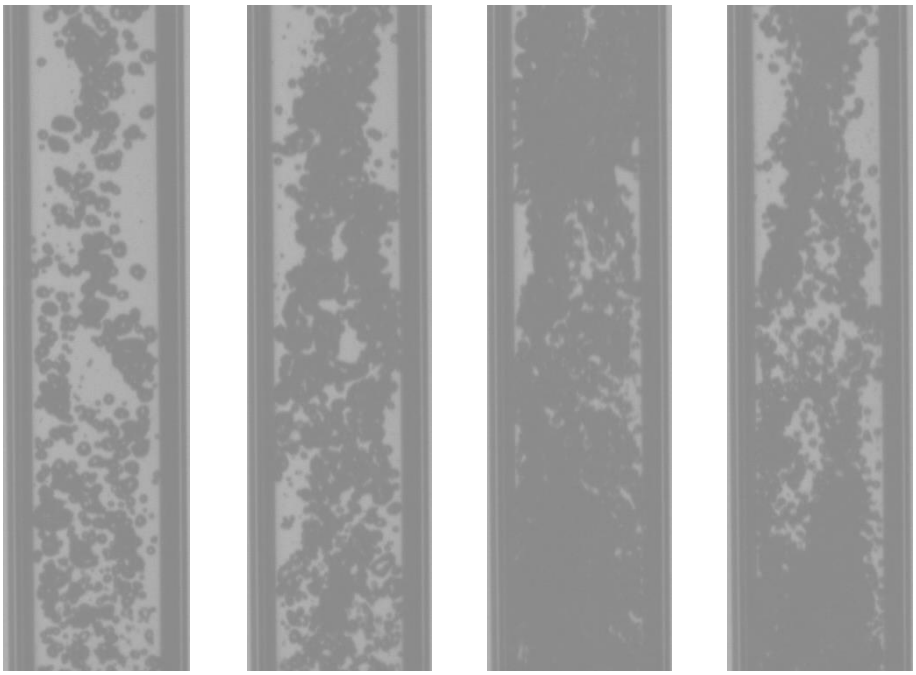

FIGURE 36 - L=942 L/H, CAC, IN ORDER LEFT TO RIGHT, G_1=1,52 L/MIN, G_2=7,38 L/MIN, G_3=19,71 L/MIN, BUBBLE ENTRAINMENT AREA WITH G_3.

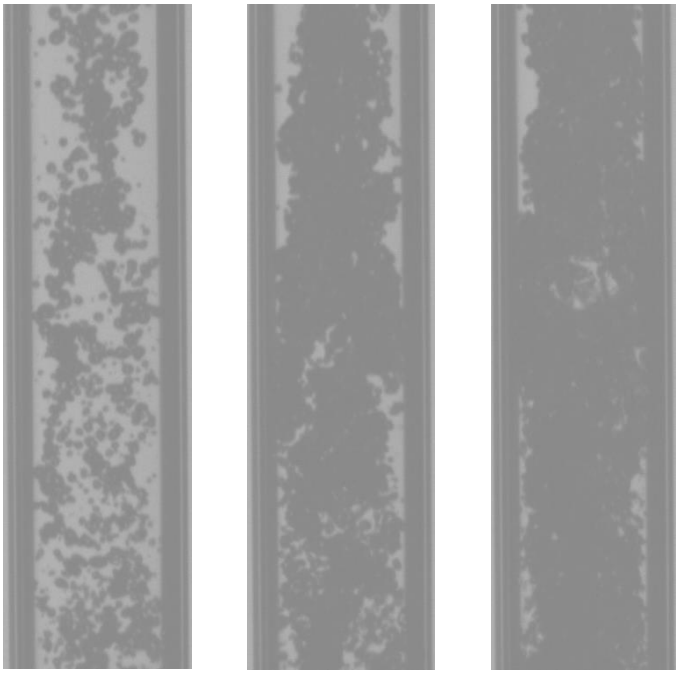

FIGURE 37 - L=1368 L/H, CAC, IN ORDER LEFT TO RIGHT, G_1=1,52 L/MIN, G_2=7,38 L/MIN, G_3=19,71 L/MIN.

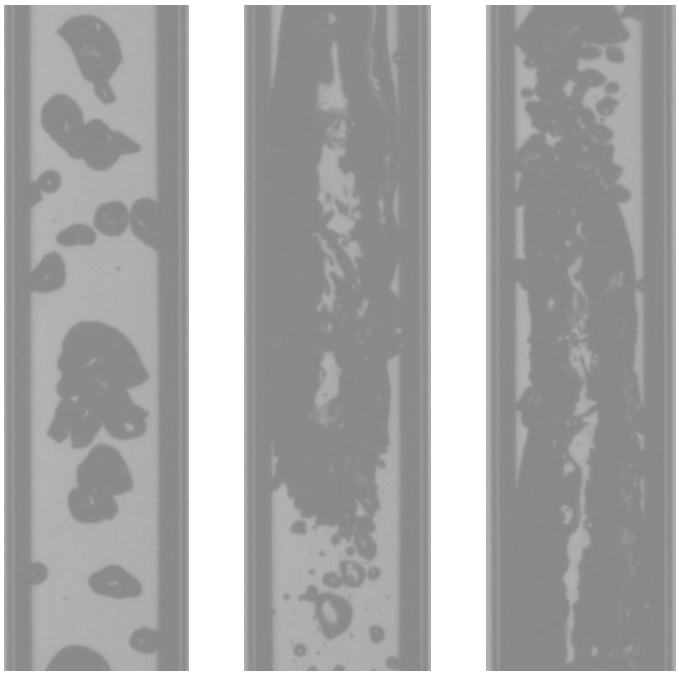

FIGURE 38 - L=455 L/H, CCC, IN ORDER LEFT TO RIGHT, G_1=1,52 L/MIN, G_2=7,38 L/MIN, G_3=19,71 L/MIN.

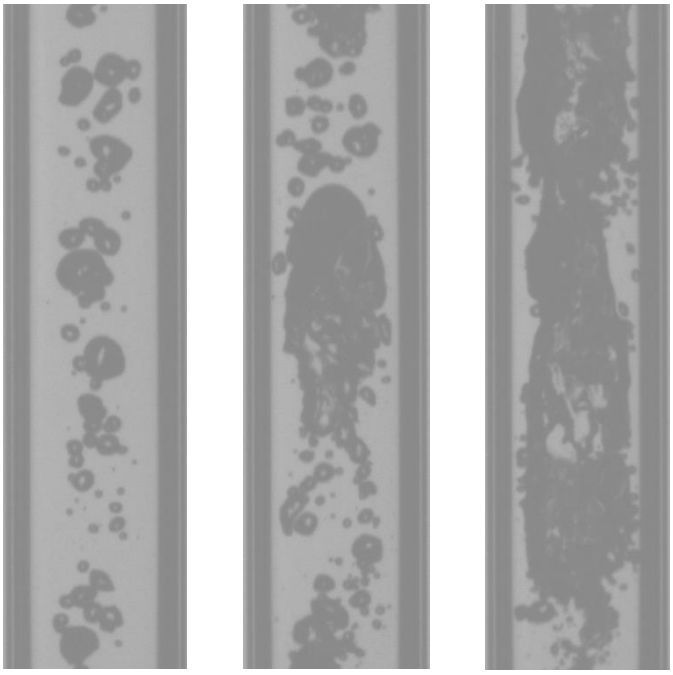

FIGURE 39 - L=942 L/H, CCC, IN ORDER LEFT TO RIGHT, G_1=1,52 L/MIN, G_2=7,38 L/MIN, G_3=19,71 L/MIN.

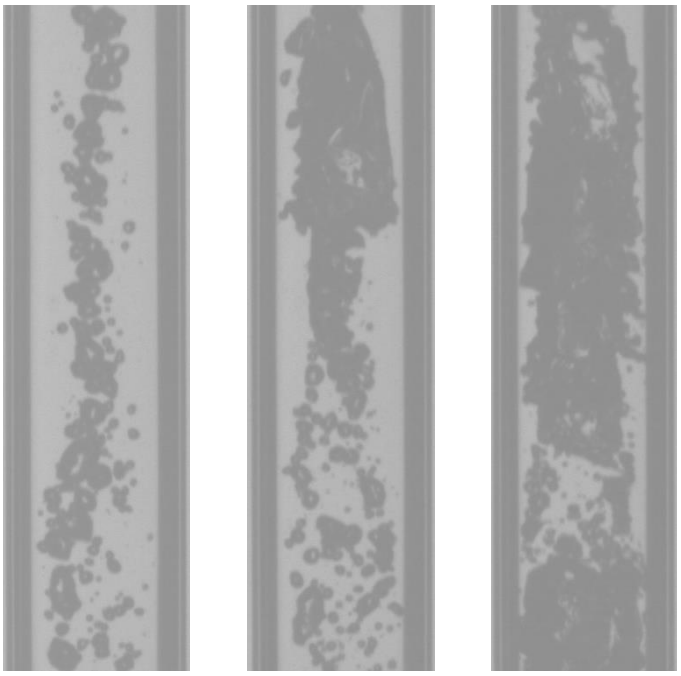

FIGURE 40 - L=1368 L/H, CCC, IN ORDER LEFT TO RIGHT, G_1=1,52 L/MIN, G_2=7,38 L/MIN, G_3=19,71 L/MIN.

The occupancy map, i.e. where the gas is located in the pipe, is clear and unambiguous.

This is experimental evidence that as conditions change, i.e. gas flow rate, liquid flow rate and static mixers, the practical effects are different.

At low gas and liquid flow rates, the bubbles are small and flow discontinuously. In fact, at flow rate L=455 L/h, G=1,52 L/min, it is possible to see a discontinuous movement of the bubbles and the effects of the static mixers are very evident: with CCC the bubbles are directed towards the inside of the tube, with CAC instead they are distributed towards the walls. With the higher liquid flow rate, this effect is visually very obvious.

As the gas flow rate increases, the bubbles become larger, but a drag zone is created, i.e. a tail of bubbles made up of many very small bubbles.

2.2 Histogram of occupancy map

A histogram is a graphical representation of a function that is continuous in nature. This is useful because it makes it possible to visualize the differences in the output of the recorded signals.

Using the MATLAB software, it was possible to do some post-processing on the data and then display it in the form of a histogram: it plots the differences in signal intensity across the frequency spectrum. In addition, the area under the function was calculated, so that a numerical value was recorded as well as a visual one.

Subtraction has been performed between two selected 'Pfinal' functions, so that on the x-axis we obtain the difference in FFT frequency intentionality, which allows us to better visualize the differences. The MATLAB code is given in *Figure 41*.

```
df1=abs(PfinalL455G1CAC-PfinalL455G1CCC);

h=histogram(df1,2500);
dhf=h.Values;

a1=trapz(dhf);
```

FIGURE 41 – MATLAB CODE FOR PLOTTING HISTOGRAM.

What is displayed, i.e. the final result, is shown in *Figure 42.*

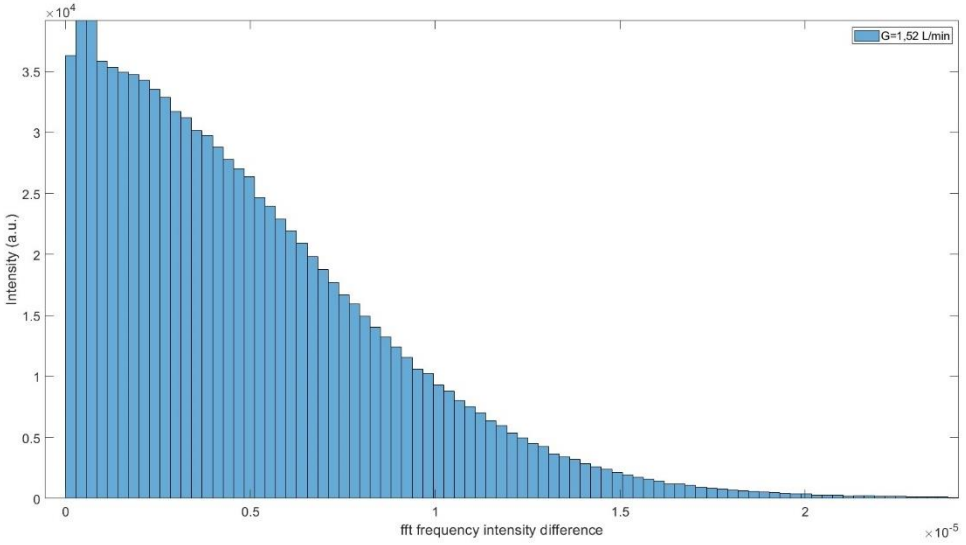

FIGURE 42 – HISTOGRAM FOR L=455 L/H, G=1,52 L/MIN.

By doing the same operation for several cases, it was then possible to compare the differences. One easy way to visualize them is to 'hold on' and an example is given to show that the differences are visible.

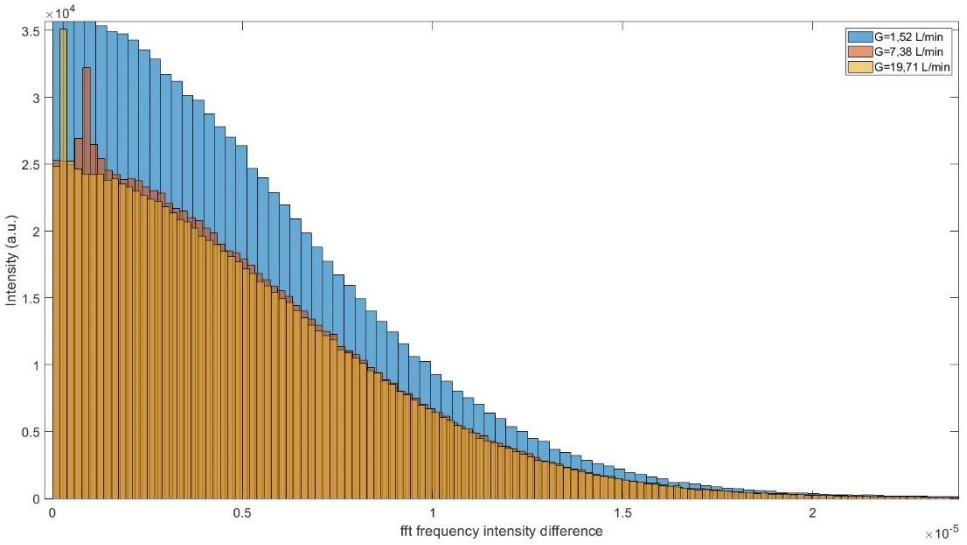

FIGURE 43 – HOLD ON OF HISTOGRAM AT THREE DIFFERENT GAS FLOW RATES.

Different conditions return different data, as it can be seen immediately in *Figure 43.*

In partcular, it is displaying the condition in which the liquid flow rate is L=455 L/h and the gas flow rates are the usual three. The difference between functions is made between the two static mixers.

3 Analysis of greyscale

In order to obtain feedback from the image data, a post-processing method based on the greyscales generated by the occupancy map in the pipe was useful.

The image data were saved as .cvc and then processed via matlab.

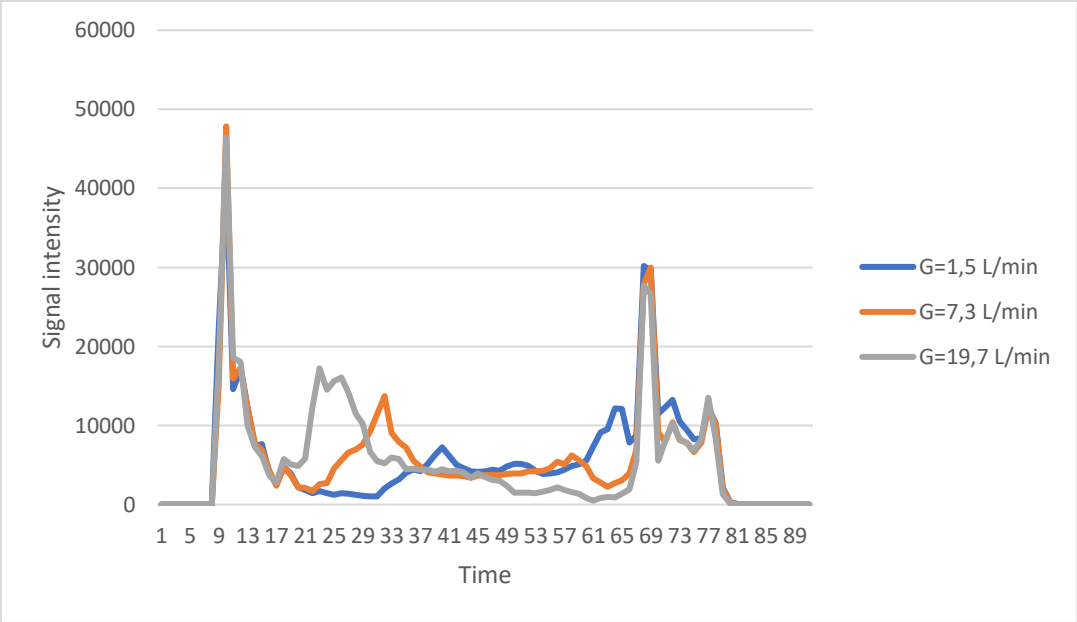

FIGURE 44 - GREY SCALE VALUES

For the purpose of comparing different conditions, the same graph illustrates the grey intensity trend at constant liquid flow rates and with identical static mixers, but with varying gas flow rates. *Figure 44* shows the grey scale trends for the following conditions:

- L=455 L/h
- Empty pipe

It can be seen that the situation inside the tube changes when the conditions are different. The end zones, however, where the signals are the same, probably refer to the pipe. That is why they remain constant.

4 Pressure drop evaluation

In order to carry out an accurate analysis of the process, it was decided to carry out a pressure drop assessment.

Using Bernulli's law, it was possible to calculate the theoretical pressure drop and compare it with the pressure drop measured by the instrument.

Below is a table showing the state in which the system was in a given analysis and, next to it, the pressure values, the theoretical and the actual ones.

All differences were made by taking as a reference, or 'zero', the pressure in the pipe under static conditions, i.e. with the pump switched off and the pipe filled with water.

System	Teoric loss	Real loss
L=455 L/h, empty	0,0014 bar	0,027 bar
L=942 L/h, empty	0,012 bar	0,030 bar
L=1365 L/h, empty	0,013 bar	0,011 bar
L=455 L/h, CAC	0,0069 bar	0,028 bar
L=942 L/h, CAC	0,029 bar	0,028 bar
L=1365 L/h, CAC	0,063 bar	0,061 bar
L=455 L/h, CCC	0,0042 bar	0,034 bar
L=942 L/h, CCC	0,018 bar	0,.37 bar
L=1365 L/h, CCC	0,038 bar	0,065 bar

TABLE 4 – VALORS OF PRESSURE DROP.

The measured pressure losses are in agreement with the theoretical ones. The losses below 0.01 bar are not of the same order of magnitude as the real ones, but this is considered to be the limit of detectability of the instrument.

Appendix

1. Passive acoustic measurement results

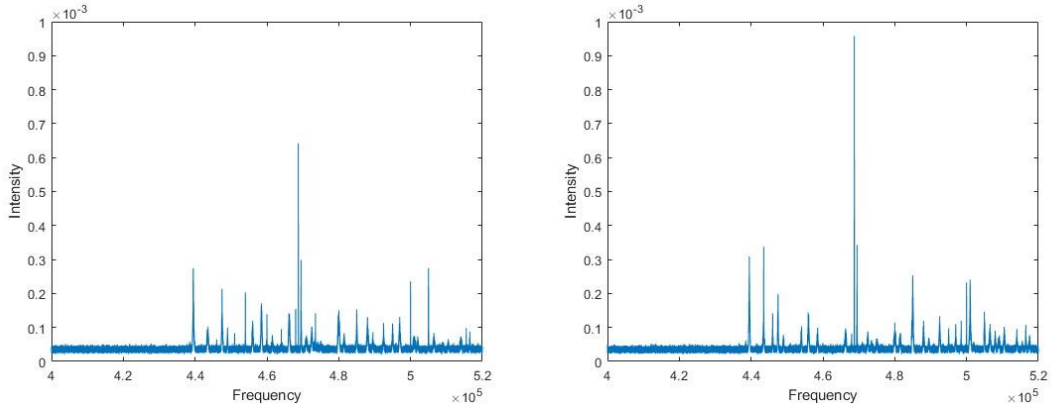

FIGURE 45 - INTENSITY VS. FREQUENCY FOR L=455 L/H, G=7,38 L/MIN, LEFT WITH EMPTY PIPE, RIGHT WITH CCC STATIC MIXERS.

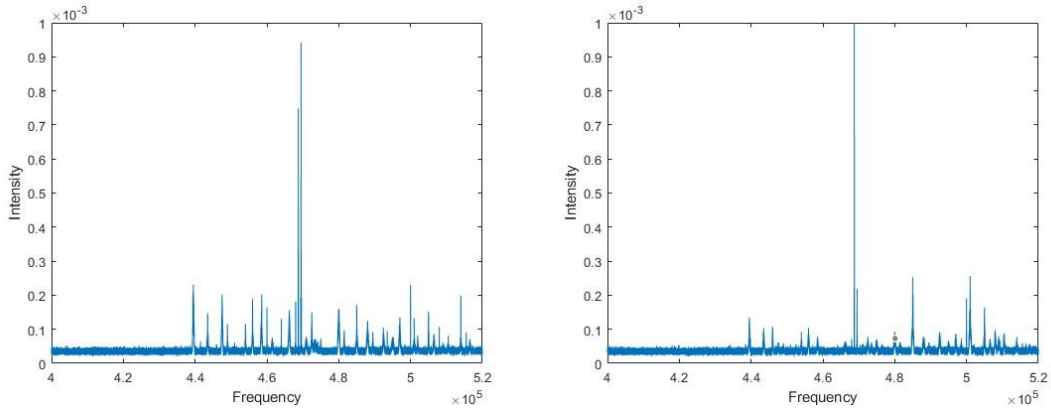

FIGURE 46 - INTENSITY VS. FREQUENCY FOR L=455 L/H, G=19,71 L/MIN, LEFT WITH EMPTY PIPE, RIGHT WITH CAC STATIC MIXERS.

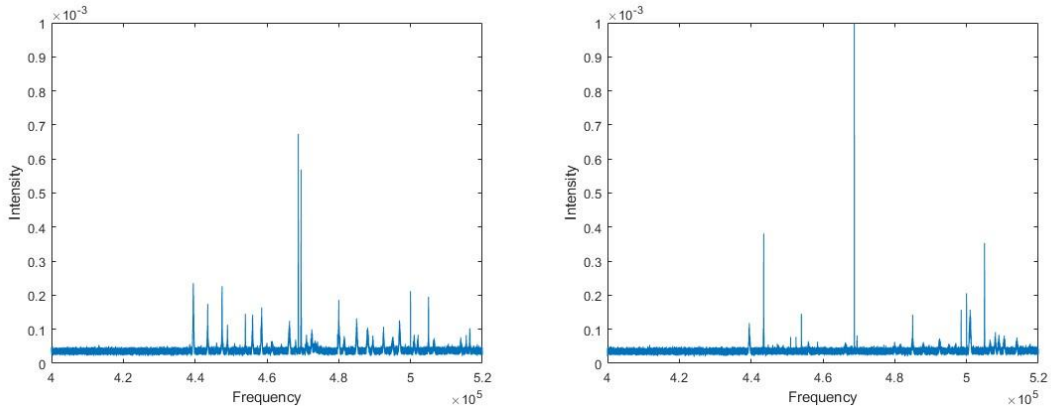

FIGURE 47 - INTENSITY VS. FREQUENCY FOR L=942 L/H, G=1,52 L/MIN, LEFT WITH EMPTY PIPE, RIGHT WITH CCC STATIC MIXERS.

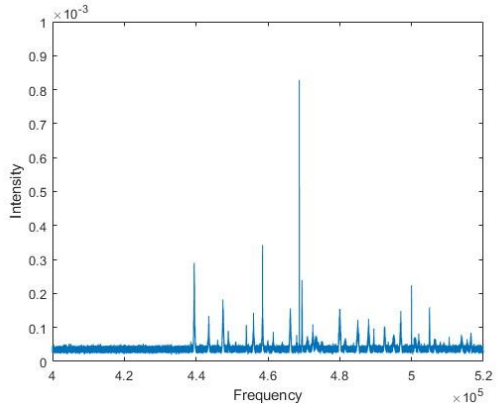

FIGURE 48 - INTENSITY VS. FREQUENCY FOR L=942 L/H, G=7,38 L/MIN, EMPTY PIPE.

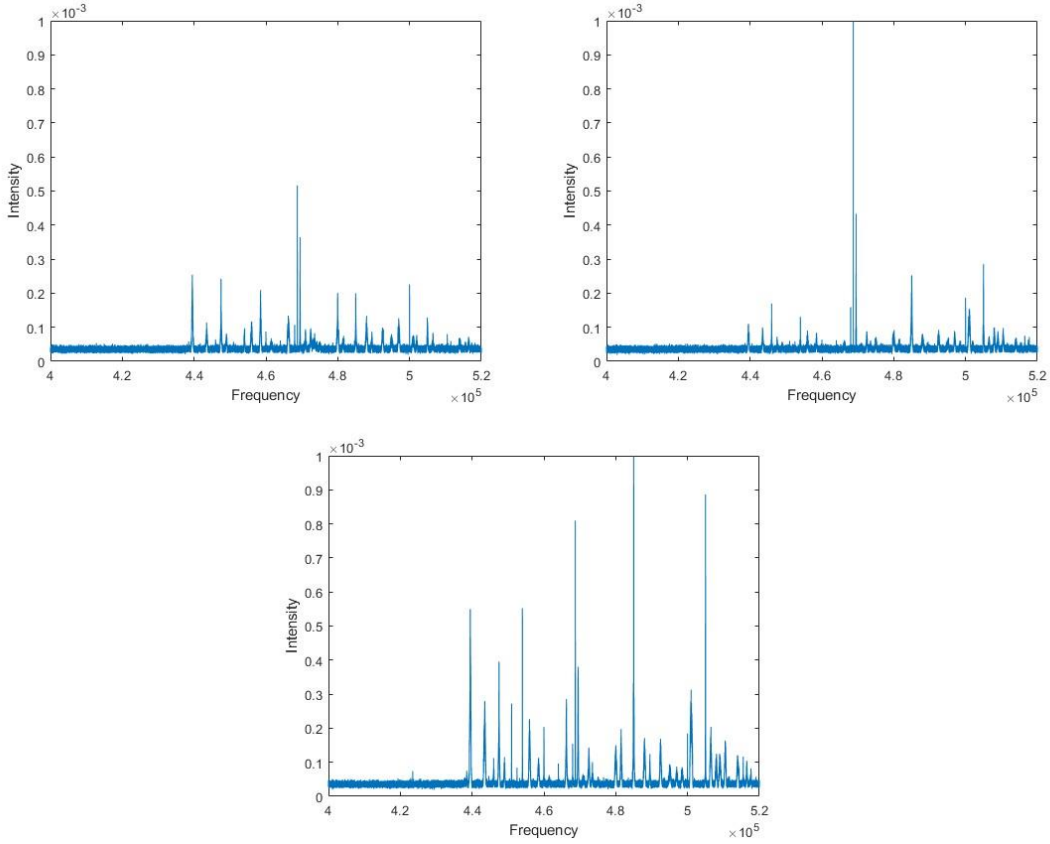

FIGURE 49 - INTENSITY VS. FREQUENCY FOR L=942 L/H, G=19,71 L/MIN, FROM RIGHT TO LEFT, EMPTY PIPE, WITH CAC AND CCC STATIC MIXERS.

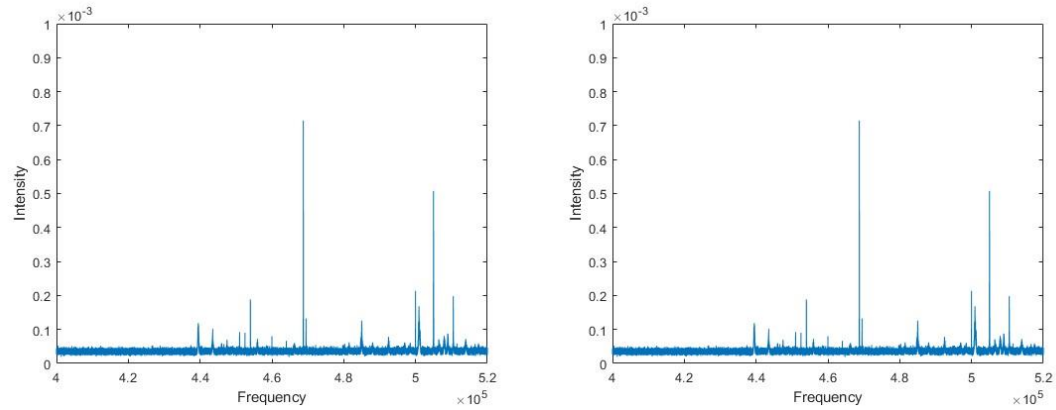

FIGURE 50 - INTENSITY VS. FREQUENCY FOR L=1368 L/H, G=1,52 L/MIN, LEFT WITH EMPTY PIPE, RIGHT WITH CCC STATIC MIXERS.

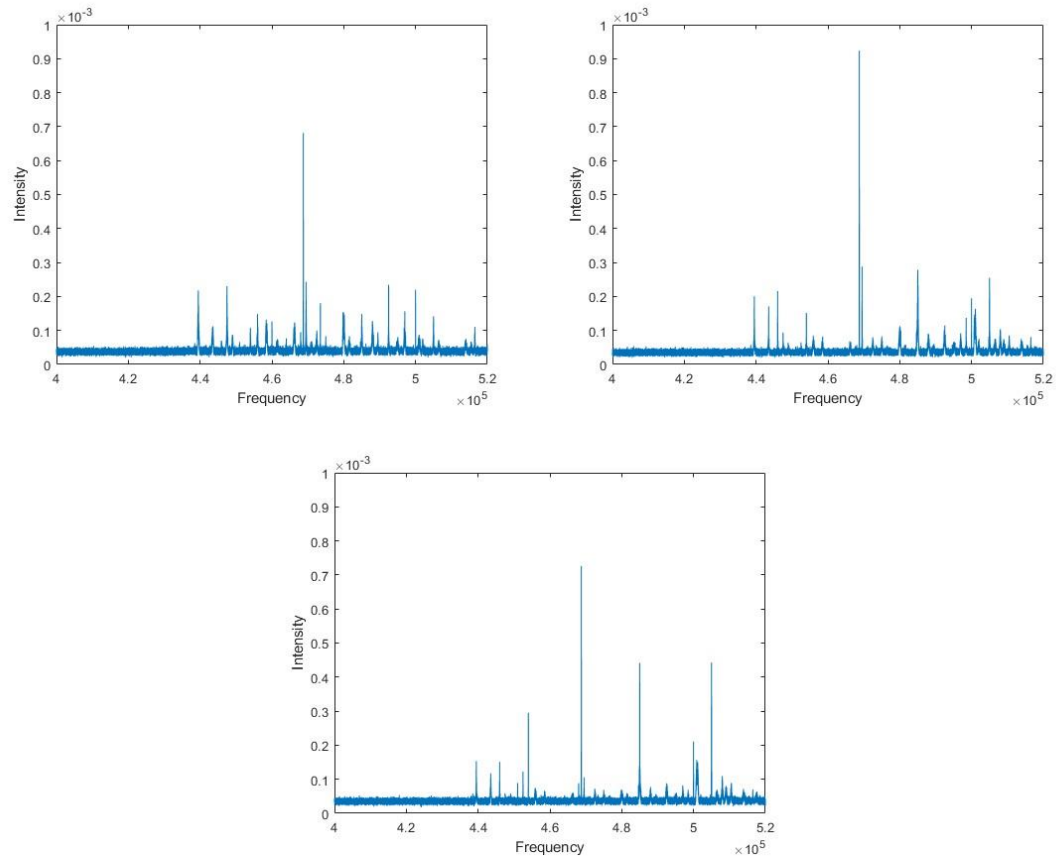

FIGURE 51 - INTENSITY VS. FREQUENCY FOR L=1368 L/H, G=19,71 L/MIN, FROM RIGHT TO LEFT, EMPTY PIPE, WITH CAC AND CCC STATIC MIXERS.

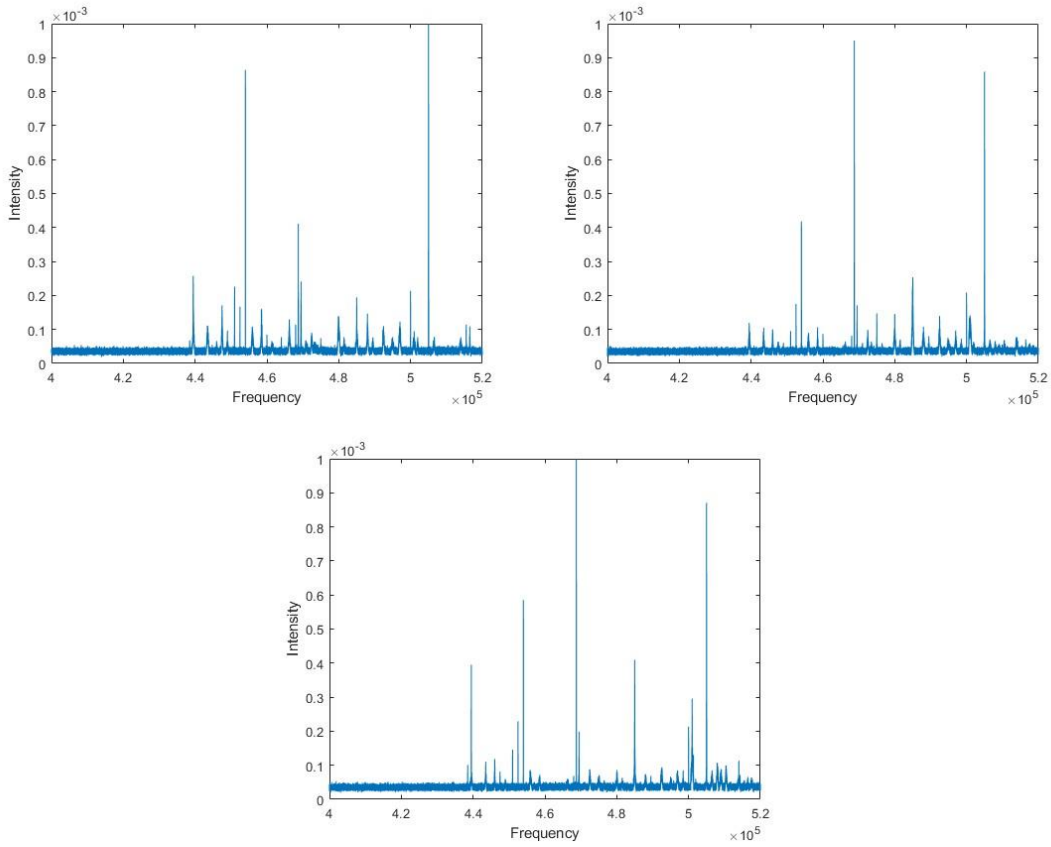

FIGURE 52 - - INTENSITY VS. FREQUENCY FOR L=1368 L/H, G=19,71 L/MIN, FROM RIGHT TO LEFT, EMPTY PIPE, WITH CAC AND CCC STATIC MIXERS.

2. Grey scale analysis

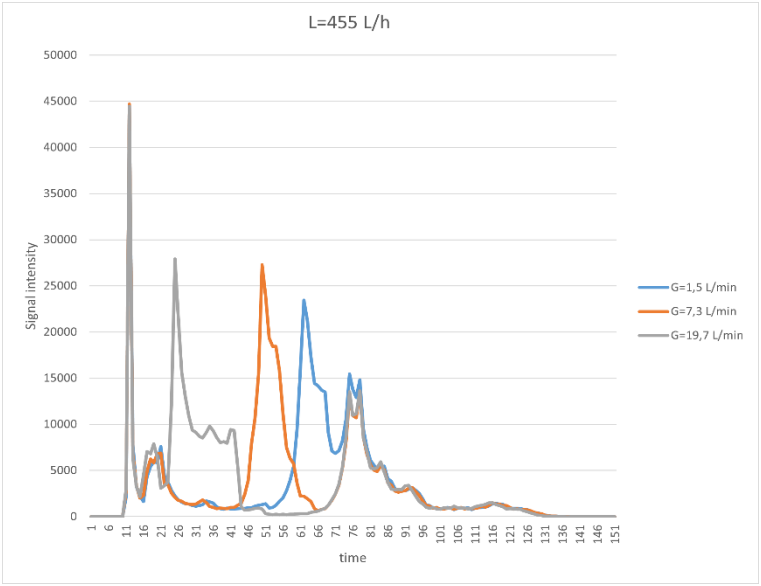

FIGURE 53 - GREY SCALE VALUES, EMPTY PIPE

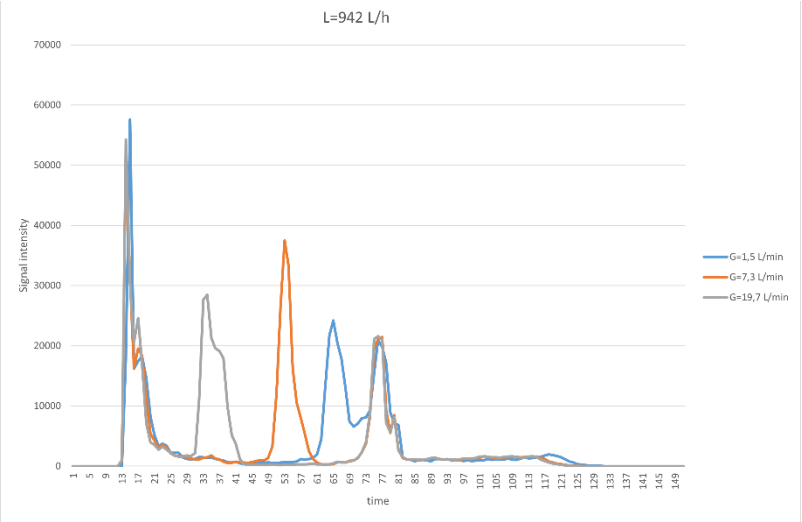

FIGURE 54 - GREY SCALE VALUES, EMPTY PIPE

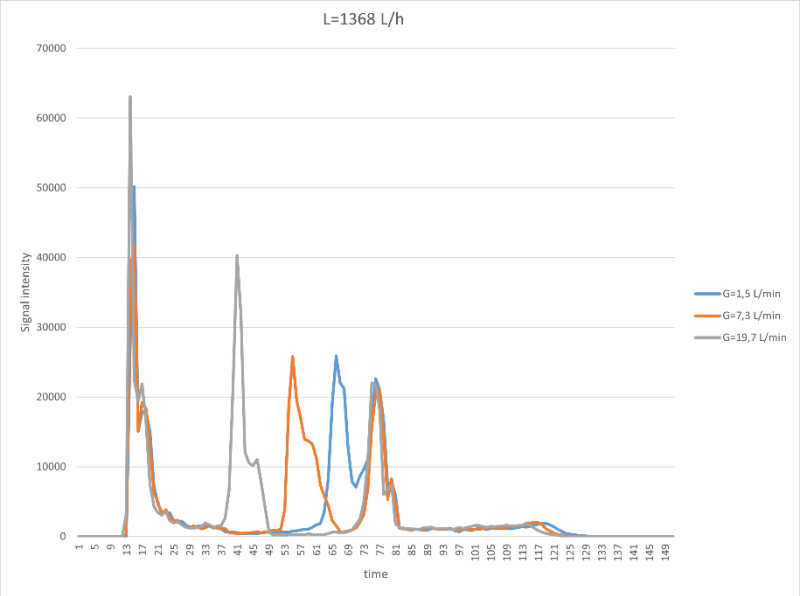

FIGURE 55 - GREY SCALE VALUES, EMPTY PIPE

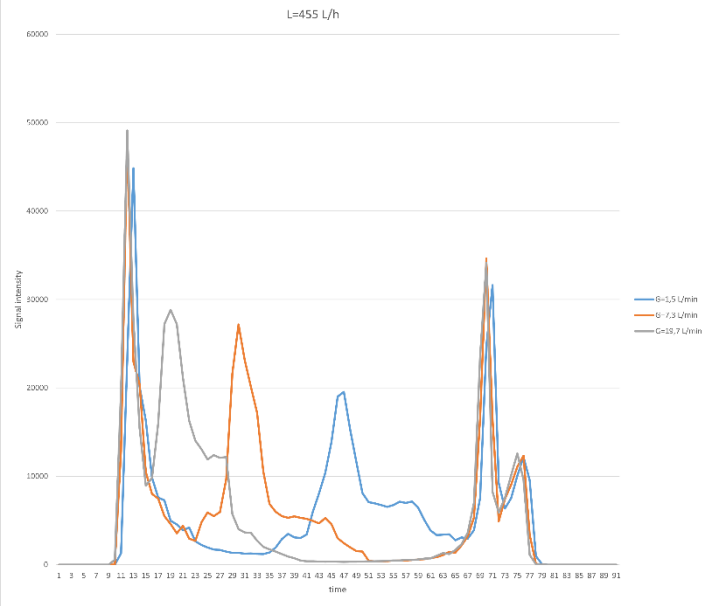

FIGURE 56 - GREY SCALE VALUES, CAC

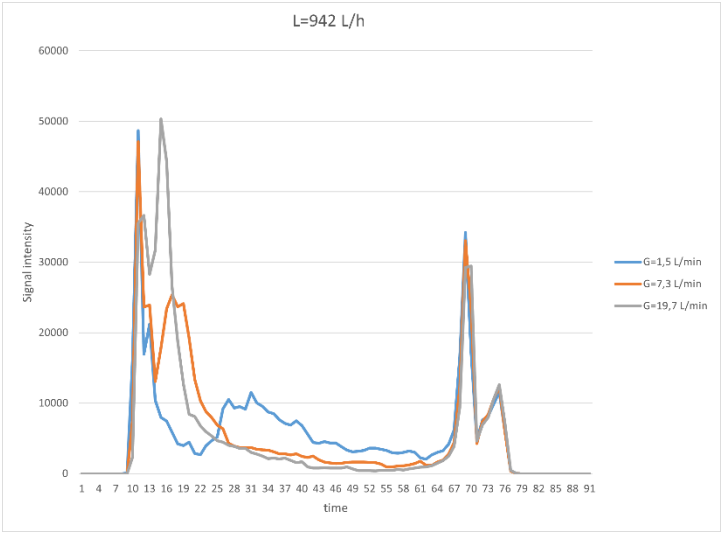

FIGURE 57 - GREY SCALE VALUES, CAC

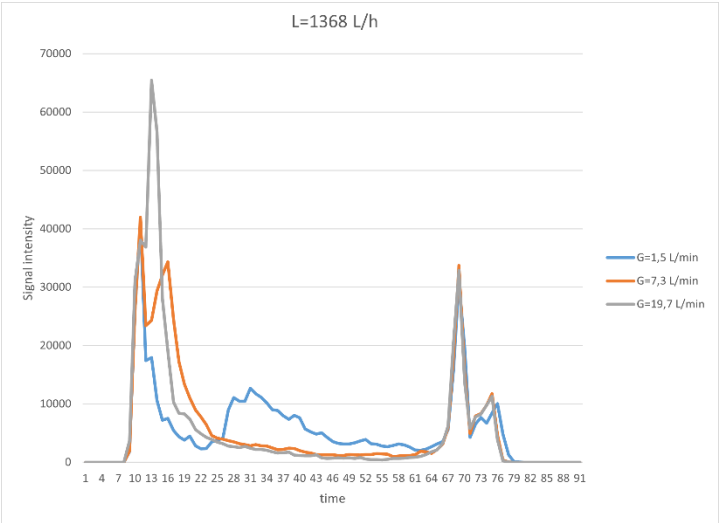

FIGURE 58 - GREY SCALE VALUES, CAC

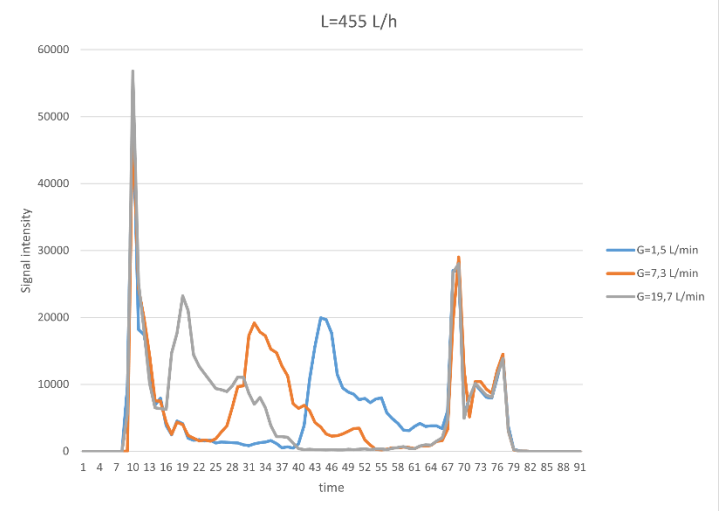

FIGURE 59 - GREY SCALE VALUES, CAC

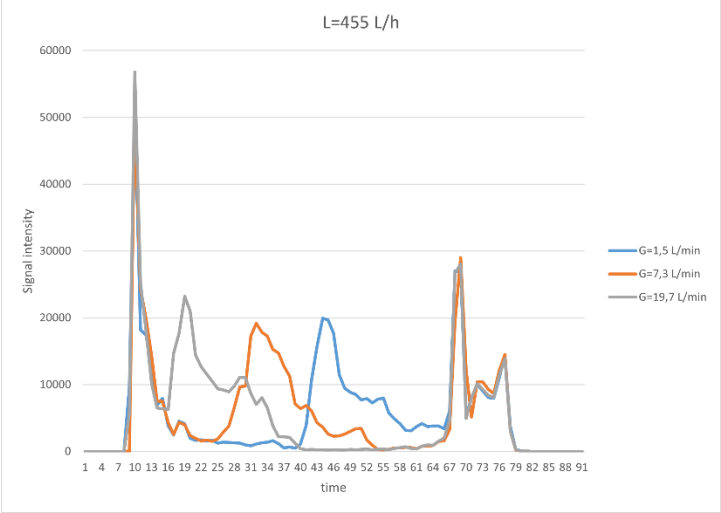

FIGURE 60 - GREY SCALE VALUES, CCC

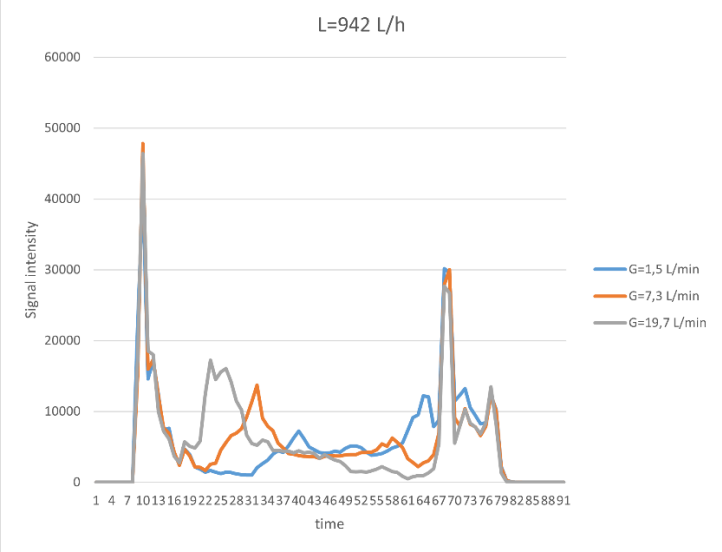

FIGURE 61 - GREY SCALE VALUES, CCC

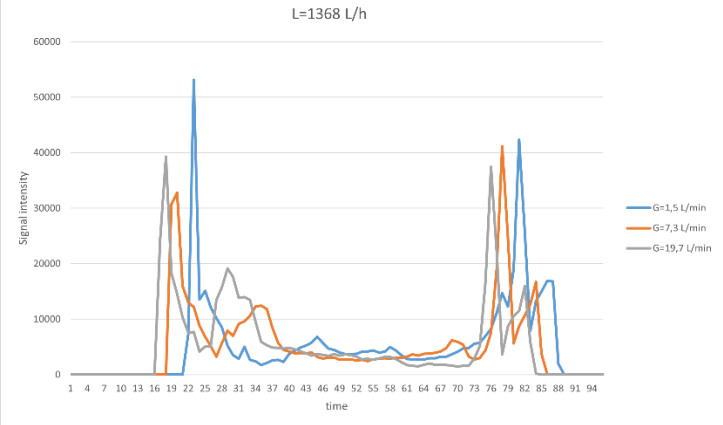

FIGURE 62 - GREY SCALE VALUES, CCC

3. Pressure measurement

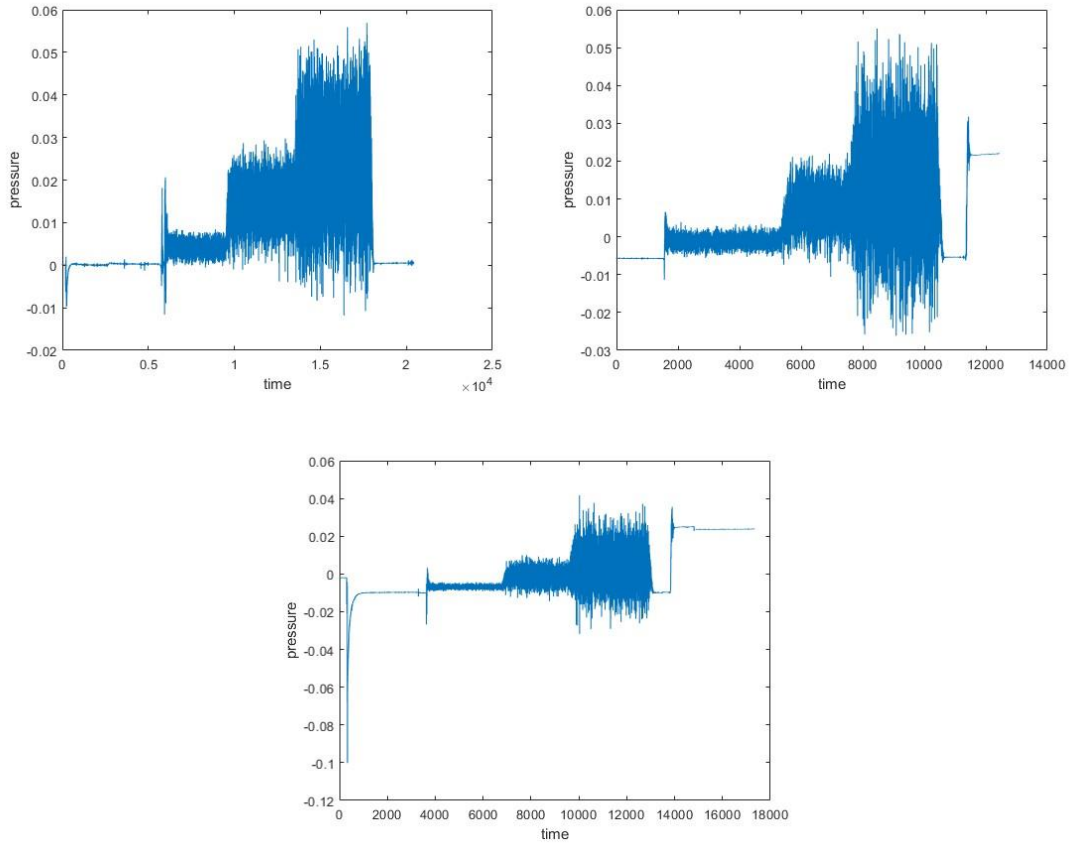

FIGURE 63 – PRESSURE MEASURED FOR L=455 L/H , INCREASING GAS FLOW, IN ORDER, EMPTY PIPE, CAC, CCC

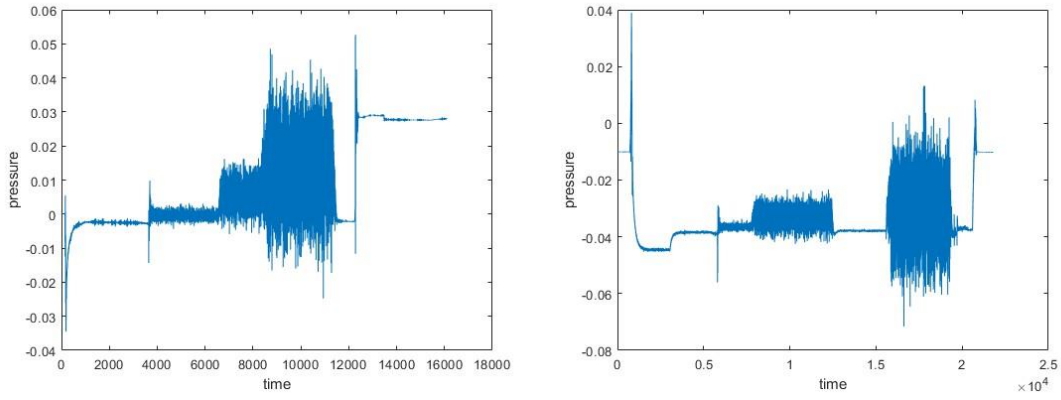

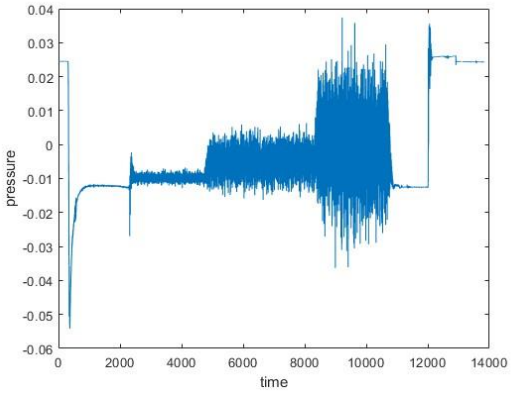

FIGURE 64 – PRESSURE MEASURED FOR L=942 L/H , INCREASING GAS FLOW, IN ORDER, EMPTY PIPE, CAC, CCC

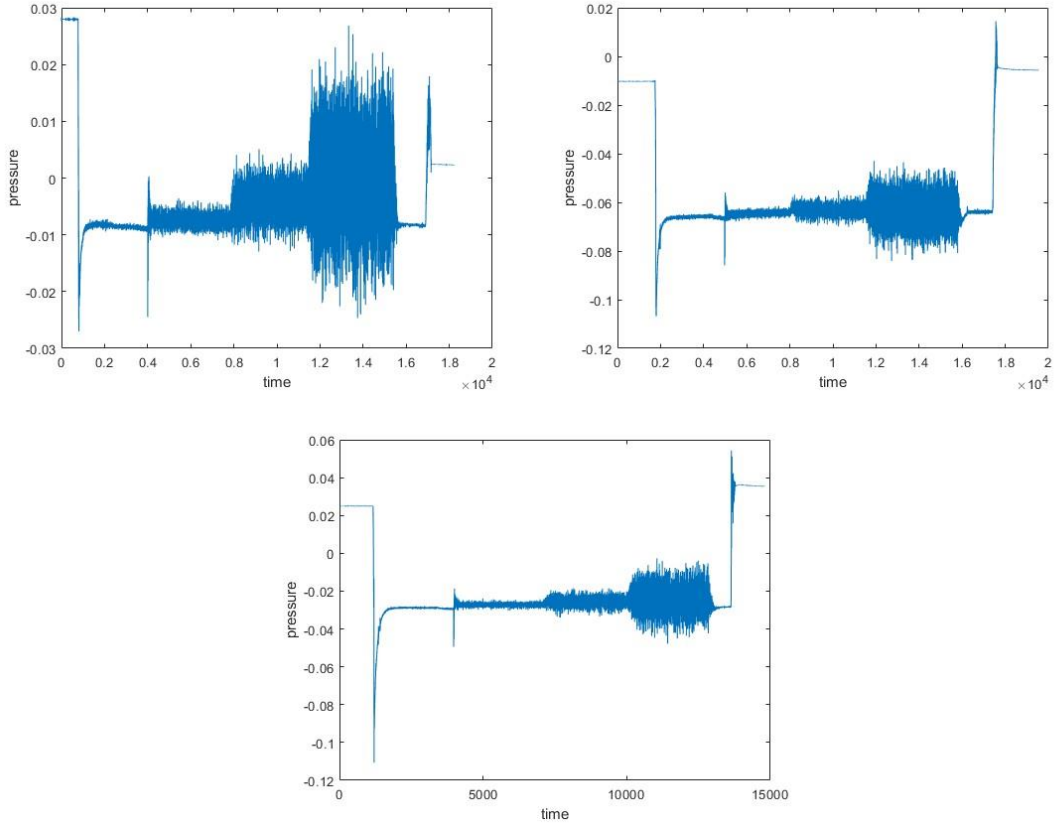

FIGURE 65 PRESSURE MEASURED FOR L=1368 L/H , INCREASING GAS FLOW, IN ORDER, EMPTY PIPE, CAC, CCC

Conclusions

This project has studied the effectiveness of passive acoustic monitoring as a valid technique for the detection and characterisation of the presence of gas-liquid phases in a plug flow reactor.

A correlation between acoustic signals and the dispersion of the gas into the liquid phase in the reactor could be observed, highlighting the potential for real-time monitoring and control in industrial processes.

Thanks to the images recorded using a camera and the data processing carried out with the DynamicStudio and MATLAB software, it was possible to monitor the concrete differences within the pipe generate by the chosen gas and liquid flow rates adopted and the presence of the static mixers.

This project demonstrated the effectiveness of passive acoustic monitoring as a valid technique to detect and characterize the presence of gas-liquid phases in a plug flow reactor.

The implementation of passive acoustic sensors provides a non-invasive and cost-effective solution for flow monitoring.

Future work could focus on further refining the acoustic data processing algorithms and integrating this technique with the use of the images to develop a predictive model.

Passive acoustic monitoring represents a promising advancement in process monitoring technology, offering a robust tool for the detection and analysis of gas-liquid phases in plug flow reactors. This project has laid the foundation for further development and industrial application of this innovative approach.

References

1. Cfr. F. Montagnaro, slide del corso di Impianti Chimici, Università degli studi di Napoli, 2020.
2. Banaga AB, Li YB, Li ZH, Sun BC, Chu GW. Experimental investigation of the mixing efficiency via intensity of segregation along axial direction of a rotating bar reactor. *Chin J Chem Eng*. 2023;59:153-159. doi:10.1016/j.cjche.2023.01.003
3. Felder1 RM, Hill FB. *Mixing Effects in Chemical Reactors*. Vol 9. UTC; 1970. https://pubs.acs.org/sharingguidelines
4. Felder RM, Rousseau RW. *ELEMENTARY PRINCIPLES OF CHEMICAL PROCESSES 2005 Edition with Integrated Media and Study Tools*.
5. Cavani F, Centi G, Di Serio M, Rossetti I, Salvini A, Strukul G. *Fondamenti Di Chimica Industriale*.
6. Yeh AC, Bai H. Comparison of ammonia and monoethanolamine solvents to reduce CO2 greenhouse gas emissions. *Science of The Total Environment*. 1999;228(2-3):121-133. doi:10.1016/S0048-9697(99)00025-X
7. Holloway S. Underground sequestration of carbon dioxide—a viable greenhouse gas mitigation option. *Energy*. 2005;30(11-12):2318-2333. doi:10.1016/j.energy.2003.10.023
8. Yang ZZ, He LN, Gao J, Liu AH, Yu B. Carbon dioxide utilization with C–N bond formation: carbon dioxide capture and subsequent conversion. *Energy Environ Sci*. 2012;5(5):6602. doi:10.1039/c2ee02774g
9. Bandyopadhyay A. Amine versus ammonia absorption of CO2 as a measure of reducing GHG emission: a critical analysis. *Clean Technol Environ Policy*. 2011;13(2):269-294. doi:10.1007/s10098-010-0299-z
10. Kang D, Park S, Jo H, Park J. Carbon fixation using calcium oxide by an aqueous approach at moderate conditions. *Chemical Engineering Journal*. 2014;248:200-207. doi:10.1016/j.cej.2014.03.045
11. Ma S, Song H, Wang M, Yang J, Zang B. Research on mechanism of ammonia escaping and control in the process of CO2 capture using ammonia solution. *Chemical Engineering Research and Design*. 2013;91(7):1327-1334. doi:10.1016/j.cherd.2013.01.020
12. Park S, Lee MG, Park J. CO2 (carbon dioxide) fixation by applying new chemical absorption-precipitation methods. *Energy*. 2013;59:737-742. doi:10.1016/j.energy.2013.07.057
13. Ind. Eng. Chem. Res. 2016, 55, 45, 11795-11800.
14. Lee MG, Kang D, Yoo Y, Jo H, Song HJ, Park J. Continuous and Simultaneous CO_2 Absorption, Calcium Extraction, and Production of Calcium Carbonate Using Ammonium Nitrate. *Ind Eng Chem Res*. 2016;55(45):11795-11800. doi:10.1021/acs.iecr.6b02880
15. Olajire AA. CO2 capture and separation technologies for end-of-pipe applications – A review. *Energy*. 2010;35(6):2610-2628. doi:10.1016/j.energy.2010.02.030
16. Global climate strike. *Nat Catal*. 2019;2(10):831-831. doi:10.1038/s41929-019-0374-8
17. Bandyopadhyay A. Amine versus ammonia absorption of CO2 as a measure of reducing GHG emission: a critical analysis. *Clean Technol Environ Policy*. 2011;13(2):269-294. doi:10.1007/s10098-010-0299-z

18. Budget, G., 2023. Global Carbon Budget 2023, Global Carbon Budget. United Kingdom. https://policycommons.net/artifacts/9769109/essd-15-5301-2023/10658360/ on 13 Jan 2024. CID: 20.500.12592/crjdj38.

19. United Nations. https://unfccc.int/process-and-meetings/the-paris-agreement.

20. International Renewable Energy Agency. Perspectives for the energy transition: Investment needs for a low-carbon energy system, https://www.irena.org/publications/2017/Mar/Perspectives-for-the-energy-transition-Investment-needs-for-a-low-carbon-energy-system.

21. www.irena.org. Energy Agency, I. & Renewable Energy Agency, I. PERSPECTIVES FOR THE ENERGY TRANSITION Investment Needs for a Low-Carbon Energy System.

22. Wilberforce T, Olabi AG, Sayed ET, Elsaid K, Abdelkareem MA. Progress in carbon capture technologies. *Science of The Total Environment*. 2021;761:143203. doi:10.1016/j.scitotenv.2020.143203

23. Theo WL, Lim JS, Hashim H, Mustaffa AA, Ho WS. Review of pre-combustion capture and ionic liquid in carbon capture and storage. *Appl Energy*. 2016;183:1633-1663. doi:10.1016/j.apenergy.2016.09.103

24. Wang M, Yao L, Wang J, et al. Adsorption and regeneration study of polyethylenimine-impregnated millimeter-sized mesoporous carbon spheres for post-combustion CO2 capture. *Appl Energy*. 2016;168:282-290. doi:10.1016/j.apenergy.2016.01.085

25. *Https://Earth.Yale.Edu/Sites/Default/Files/Files/Bui_Thesis.Pdf*.

26. Plaza MG, González AS, Pevida C, Pis JJ, Rubiera F. Valorisation of spent coffee grounds as CO2 adsorbents for postcombustion capture applications. *Appl Energy*. 2012;99:272-279. doi:10.1016/j.apenergy.2012.05.028

27. Kolle JM, Fayaz M, Sayari A. Understanding the Effect of Water on CO_2 Adsorption. *Chem Rev*. 2021;121(13):7280-7345. doi:10.1021/acs.chemrev.0c00762

28. Lai JY, Ngu LH, Hashim SS. A review of CO_2 adsorbents performance for different carbon capture technology processes conditions. *Greenhouse Gases: Science and Technology*. 2021;11(5):1076-1117. doi:10.1002/ghg.2112

29. Presser V, McDonough J, Yeon SH, Gogotsi Y. Effect of pore size on carbon dioxide sorption by carbide derived carbon. *Energy Environ Sci*. 2011;4(8):3059. doi:10.1039/c1ee01176f

30. Kumar S, Srivastava R, Koh J. Utilization of zeolites as CO2 capturing agents: Advances and future perspectives. *Journal of CO2 Utilization*. 2020;41:101251. doi:10.1016/j.jcou.2020.101251

31. https://www.docenti.unina.it/webdocenti-be/allegati/materiale-didattico/77473.

32. Aaron D, Tsouris C. Separation of CO_2 from Flue Gas: A Review. *Sep Sci Technol*. 2005;40(1-3):321-348. doi:10.1081/SS-200042244

33. Elhajj J, Al-Hindi M, Azizi F. A Review of the Absorption and Desorption Processes of Carbon Dioxide in Water Systems. *Ind Eng Chem Res*. 2014;53(1):2-22. doi:10.1021/ie403245p

34. Knoche W. Chemical Reactions of CO2 in Water. In: ; 1980:3-11. doi:10.1007/978-3-642-67572-0_1

35. Bui M, Adjiman CS, Bardow A, et al. Carbon capture and storage (CCS): the way forward. *Energy Environ Sci*. 2018;11(5):1062-1176. doi:10.1039/C7EE02342A

36. Abed R, Hussein MM, Ahmed WH, Abdou S. Two-Phase Flow Mass Transfer Analysis of Airlift Pump for Aquaculture Applications. *Fluids*. 2021;6(6):226. doi:10.3390/fluids6060226

37. Doucette A, Holagh SG, Ahmed WH. CO2 capture using gas-lift pumps operating under two-phase flow conditions. *Int J Heat Mass Transf*. 2024;224:125374. doi:10.1016/j.ijheatmasstransfer.2024.125374

38. Alberini F, Bezchi D, Mannino IC, Paglianti A, Montante G. Towards real time monitoring of reacting species and pH coupling electrical resistance tomography and machine learning methodologies. *Chemical Engineering Research and Design*. 2021;168:369-382. doi:10.1016/j.cherd.2021.02.024

39. https://tuvaustriaitalia.com/testing/cose-lemissione-acustica/.

40. McClements DJ, Gunasekaran S. Ultrasonic characterization of foods and drinks: Principles, methods, and applications. *Crit Rev Food Sci Nutr*. 1997;37(1):1-46. doi:10.1080/10408399709527766

41. Nordon A, Waddell RJH, Bellamy LJ, et al. Monitoring of a heterogeneous reaction by acoustic emission. *Analyst*. 2004;129(5):463. doi:10.1039/b402875a

42. Nair A, Cai CS. Acoustic emission monitoring of bridges: Review and case studies. *Eng Struct*. 2010;32(6):1704-1714. doi:10.1016/j.engstruct.2010.02.020

43. W.R. Boyd J, Varley J. The uses of passive measurement of acoustic emissions from chemical engineering processes. *Chem Eng Sci*. 2001;56(5):1749-1767. doi:10.1016/S0009-2509(00)00540-6

44. Shepard DD, Smith KR. A new ultrasonic measurement system for the cure monitoring of thermosetting resins and composites. *Journal of thermal analysis*. 1997;49(1):95-100. doi:10.1007/BF01987425

45. Heim Weber G, Santos EN dos, Gomes DF, et al. Measurement of Gas-Phase Velocities in Two-Phase Flow Using Distributed Acoustic Sensing. *IEEE Sens J*. 2023;23(4):3597-3608. doi:10.1109/JSEN.2022.3232269

46. https://sinay.ai/en/what-is-the-difference-between-active-and-passive-acoustic/.

47. Fomalont, Ed B. “Image analysis.” Synthesis Imaging in Radio Astronomy II. Vol. 180. 1999.

48. Walke S, Mandake M, Tapre RW, Naniwadekar M, Thakar C, Jadhav SD. Image Processing in Industrial Chemical Engineering Trends and Applications. In: ; 2023:348-363. doi:10.4018/978-1-6684-8618-4.ch021

49. Zhong S, Zou X, Zhang Z, Tian H. A flexible image analysis method for measuring bubble parameters. *Chem Eng Sci*. 2016;141:143-153. doi:10.1016/j.ces.2015.10.033

50. Sujatha KT, Meeusen BGJ, Kuipers JAM, Deen NG. Experimental studies of bubbly flow in a pseudo-2D micro-structured bubble column reactor using digital image analysis. *Chem Eng Sci*. 2015;130:18-30. doi:10.1016/j.ces.2015.02.029

51. https://ai.stanford.edu/~syyeung/cvweb/tutorial1.html#:~:text=Image%20filtering%20changes%20the%20range,points%20without%20changing%20the%20colors.

52. Laurent Najman, Michel Schmitt. Watershed of a Continuous Function. Signal Processing, 1994, 38 (1), pp.99-112. ff10.1016/0165-1684(94)90059-0ff. ffhal-00622129f.

53. Huang L, Ding L, Zhou J, et al. One-step rapid quantification of SARS-CoV-2 virus particles via low-cost nanoplasmonic sensors in generic microplate reader and point-of-care device. *Biosens Bioelectron*. 2021;171:112685. doi:10.1016/j.bios.2020.112685

54. Han BG, Han BZ, Ou JP. Novel piezoresistive composite with high sensitivity to stress/strain. *Materials Science and Technology*. 2010;26(7):865-870. doi:10.1179/026708309X12454008169546

55. Chen PW, Chung DDL. Low-drying-shrinkage concrete containing carbon fibers. *Compos B Eng*. 1996;27(3-4):269-274. doi:10.1016/1359-8368(95)00020-8

56. Fu X, Chung DDL. Self-monitoring of fatigue damage in carbon fiber reinforced cement. *Cem Concr Res*. 1996;26(1):15-20. doi:10.1016/0008-8846(95)00184-0

57. Encyclopedia of Sensors and Biosensors 2023. Thermal Sensor: Thermal sensors measure the change in temperature via the change of electrical properties of sensor materials.

58. Chen HY, Chen A, Chen C. Investigation of the Impact of Infrared Sensors on Core Body Temperature Monitoring by Comparing Measurement Sites. *Sensors*. 2020;20(10):2885. doi:10.3390/s20102885

59. Rasmussen A, Zaghloul ME. In the flow with MEMS. *IEEE Circuits and Devices Magazine*. 1998;14(4):12-25. doi:10.1109/101.708474

60. Kersjes R, Eichholz J, Langerbein A, Manoli Y, Mokwa W. An integrated sensor for invasive blood-velocity measurement. *Sens Actuators A Phys*. 1993;37-38:674-678. doi:10.1016/0924-4247(93)80114-V

61. Schütze A., Helwig N., Schneider T. Sensors 4.0 – smart sensors and measurement technology enable Industry 4.0.

62. Fernández-Caramés TM, Blanco-Novoa O, Froiz-Míguez I, Fraga-Lamas P. Towards an Autonomous Industry 4.0 Warehouse: A UAV and Blockchain-Based System for Inventory and Traceability Applications in Big Data-Driven Supply Chain Management. *Sensors*. 2019;19(10):2394. doi:10.3390/s19102394

63. Whitaker M, Baker GR, Westrup J, et al. Application of acoustic emission to the monitoring and end point determination of a high shear granulation process. *Int J Pharm*. 2000;205(1-2):79-91. doi:10.1016/S0378-5173(00)00479-8

64. BRIENS L, DANIHER D, TALLEVI A. Monitoring high-shear granulation using sound and vibration measurements. *Int J Pharm*. 2007;331(1):54-60. doi:10.1016/j.ijpharm.2006.09.012

65. Daniher D, Briens L, Tallevi A. End-point detection in high-shear granulation using sound and vibration signal analysis. *Powder Technol*. 2008;181(2):130-136. doi:10.1016/j.powtec.2006.12.003

66. Gamble JF, Dennis AB, Tobyn M. Monitoring and end-point prediction of a small scale wet granulation process using acoustic emission. *Pharm Dev Technol*. 2009;14(3):299-304. doi:10.1080/10837450802603618

67. Allan P, Bellamy LJ, Nordon A, Littlejohn D. Non-invasive monitoring of the mixing of pharmaceutical powders by broadband acoustic emission. *Analyst*. 2010;135(3):518. doi:10.1039/b922446g

68. Briens L, Smith R, Briens C. Monitoring of a rotary dryer using acoustic emissions. *Powder Technol*. 2008;181(2):115-120. doi:10.1016/j.powtec.2006.12.004

69. Wang J, Yu W. Research on Hierarchy of Urban Rail Transit Hub. In: *2010 International Conference on Intelligent Computation Technology and Automation*. IEEE; 2010:1173-1176. doi:10.1109/ICICTA.2010.307

70. Matero S, Poutiainen S, Leskinen J, et al. The feasibility of using acoustic emissions for monitoring of fluidized bed granulation. *Chemometrics and Intelligent Laboratory Systems*. 2009;97(1):75-81. doi:10.1016/j.chemolab.2008.11.001

71. Zhou Y, Dong K, Zhengliang H, Wang J, Yang Y. Fault Detection Based on Acoustic Emission–Early Agglomeration Recognition System in Fluidized Bed Reactor. *Ind Eng Chem Res*. 2011;50(14):8476-8484. doi:10.1021/ie200260t

72. Flåten GR, Belchamber R, Collins M, Walmsley AD. Caterpillar—an adaptive algorithm for detecting process changes from acoustic emission signals. *Anal Chim Acta*. 2005;544(1-2):280-291. doi:10.1016/j.aca.2004.12.043

73. Nordon A, Waddell RJH, Bellamy LJ, et al. Monitoring of a heterogeneous reaction by acoustic emission. *Analyst*. 2004;129(5):463. doi:10.1039/b402875a

74. Nordon A, Carella Y, Gachagan A, Littlejohn D, Hayward G. Factors affecting broadband acoustic emission measurements of a heterogeneous reaction. *Analyst*. 2006;131(2):323-330. doi:10.1039/B510922A

75. Wentzell PD, Wade AP. Chemical acoustic emission analysis in the frequency domain. *Anal Chem*. 1989;61(23):2638-2642. doi:10.1021/ac00198a010

76. Cao Z, Wang BF, Wang KM, Lin HG, Yu RQ. Chemical acoustic emissions from gas evolution processes recorded by a piezoelectric transducer. *Sens Actuators B Chem*. 1998;50(1):27-37. doi:10.1016/S0925-4005(98)00152-X

77. Betteridge D, Joslin MT, Lilley Trevor. Acoustic emissions from chemical reactions. *Anal Chem*. 1981;53(7):1064-1073. doi:10.1021/ac00230a033

78. Esbensen KH, Halstensen M, Tønnesen Lied T, et al. Acoustic chemometrics—from noise to information. *Chemometrics and Intelligent Laboratory Systems*. 1998;44(1-2):61-76. doi:10.1016/S0169-7439(98)00114-2

79. Huang J, Ose S, de Silva S, Esbensen KH. Non-invasive monitoring of powder breakage during pneumatic transportation using acoustic chemometrics. *Powder Technol*. 2003;129(1-3):130-138. doi:10.1016/S0032-5910(02)00127-4

80. Albion K, Briens L, Briens C, Berruti F. Detection of the breakage of pharmaceutical tablets in pneumatic transport. *Int J Pharm*. 2006;322(1-2):119-129. doi:10.1016/j.ijpharm.2006.05.039

81. Albion K, Briens L, Briens C, Berruti F, McDougall S. Detection of oversized material in a hydrotransport slurry pipe using a non-invasive acoustic method. *Powder Technol*. 2009;190(3):361-371. doi:10.1016/j.powtec.2008.08.020

82. Paul EL, Atiemo-Obeng VA, Kresta SM, eds. *Handbook of Industrial Mixing*. Wiley; 2003. doi:10.1002/0471451452

83. Zwietering ThN. Suspending of solid particles in liquid by agitators. *Chem Eng Sci*. 1958;8(3-4):244-253. doi:10.1016/0009-2509(58)85031-9

84. Belchamber RM, Betteridge D, Collins MP, Lilley Trevor, Marczewski CZ, Wade AP. Quantitative study of acoustic emission from a model chemical process. *Anal Chem*. 1986;58(8):1873-1877. doi:10.1021/ac00121a058

85. He YJ, Wang JD, Yang YR. Resolution of structure characteristics of passive acoustic emission signals in multiphase flow system. *J Phys Conf Ser*. 2009;147:012008. doi:10.1088/1742-6596/147/1/012008

86. Hefft DI, Alberini F. A step towards the live identification of pipe obstructions with the use of passive acoustic emission and supervised machine learning. *Biosyst Eng*. 2020;191:48-59. doi:10.1016/j.biosystemseng.2019.12.015

87. Gleick PH. Water, Drought, Climate Change, and Conflict in Syria. *Weather, Climate, and Society*. 2014;6(3):331-340. doi:10.1175/WCAS-D-13-00059.1

88. Weng Q, ed. *Advances in Environmental Remote Sensing*. CRC Press; 2011. doi:10.1201/b10599

89. W.R. Boyd J, Varley J. The uses of passive measurement of acoustic emissions from chemical engineering processes. *Chem Eng Sci*. 2001;56(5):1749-1767. doi:10.1016/S0009-2509(00)00540-6

90. McBride K, Sundmacher K. Overview of Surrogate Modeling in Chemical Process Engineering. *Chemie Ingenieur Technik*. 2019;91(3):228-239. doi:10.1002/cite.201800091

91. Christopher M. Bishop. *Pattern Recognition and Machine Learning*.

92. Leonard KC, Hasan F, Sneddon HF, You F. Can Artificial Intelligence and Machine Learning Be Used to Accelerate Sustainable Chemistry and Engineering? *ACS Sustain Chem Eng*. 2021;9(18):6126-6129. doi:10.1021/acssuschemeng.1c02741

93. Dawson DK, Efford MG. Bird population density estimated from acoustic signals. *Journal of Applied Ecology*. 2009;46(6):1201-1209. doi:10.1111/j.1365-2664.2009.01731.x

94. Rhinehart TA, Chronister LM, Devlin T, Kitzes J. Acoustic localization of terrestrial wildlife: Current practices and future opportunities. *Ecol Evol*. 2020;10(13):6794-6818. doi:10.1002/ece3.6216

95. Thakur RK, Vial Ch, Nigam KDP, Nauman EB, Djelveh G. Static Mixers in the Process Industries—A Review. *Chemical Engineering Research and Design*. 2003;81(7):787-826. doi:10.1205/026387603322302968

96. Taitel Y, Barnea D, Dukler AE. Modelling flow pattern transitions for steady upward gas-liquid flow in vertical tubes. *AIChE Journal*. 1980;26(3):345-354. doi:10.1002/aic.690260304

97. Morgado AO, Miranda JM, Araújo JDP, Campos JBLM. Review on vertical gas–liquid slug flow. *International Journal of Multiphase Flow*. 2016;85:348-368. doi:10.1016/j.ijmultiphaseflow.2016.07.002

98. Barbosa JR, Govan AH, Hewitt GF. Visualisation and modelling studies of churn flow in a vertical pipe. *International Journal of Multiphase Flow*. 2001;27(12):2105-2127. doi:10.1016/S0301-9322(01)00048-9

99. Thakur RK, Vial Ch, Nigam KDP, Nauman EB, Djelveh G. Static Mixers in the Process Industries—A Review. *Chemical Engineering Research and Design*. 2003;81(7):787-826. doi:10.1205/026387603322302968

100. Yao Z, Alberini F, Montante G, Paglianti A. In-line monitoring of mixing performance for smart processes in tubular reactors. *Chemical Engineering Research and Design*. 2023;194:678-692. doi:10.1016/j.cherd.2023.05.013

101. Fagnani F, Tabacco A, Tilli P. *INTRODUZIONE ALL'ANALISI COMPLESSA E TEORIA DELLE DISTRIBUZIONI*.; 2006.

102. HELP CENTER MATLAB https://it.mathworks.com/help/matlab/ref/hold.html.

103. DYNAMICSTUDIO User's Guide.